frontiers in Earth Science

ORIGINAL RESEARCH
published: 27 January 2021
doi: 10.3389/feart.2020.596727

Morphotectonic Analysis of the East Manus Basin, Papua New Guinea

Nicholas J. Dyriw[1,2], Scott E. Bryan[1], Simon W. Richards, John M. Parianos[2], Richard J. Arculus[4] and David A. Gust[1]*

[1]School of Earth and Atmospheric Sciences, Queensland University of Technology, Brisbane, QLD, Australia, [2]Nautilus Minerals Ltd. (now Deep Sea Mining Finance Ltd.), Brisbane, QLD, Australia, [3]Independent Research Geologist, Brisbane, QLD, Australia, [4]Research School of Earth Sciences, Australian National University, Canberra, ACT, Australia

Backarc basin systems are important sites of extension leading to crustal rupture where basin development typically occurs in rifting phases (or stages) with the final successful stages identified by the formation of spreading ridges and new oceanic crust. The East Manus Basin is a young (<1 Ma), active, rapidly rifting backarc basin in a complex tectonic setting at the confluence of the oblique convergence of the Australian and Pacific plates. Here we undertake the first comprehensive spatial-temporal morphotectonic description and interpretation of the East Manus Basin including a link to the timing of, and tectonic controls on, the formation of seafloor massive sulfide mineralization. Key seafloor datasets used in the morphotectonic analysis include multi-resolution multibeam echosounder seafloor data and derivatives. Morphotectonic analysis of these data defines three evolutionary phases for the East Manus Basin. Each phase is distinguished by a variation in seafloor characteristics, volcano morphology and structural features: Phase 1 is a period of incipient extension of existing arc crust with intermediate to silicic volcanism; Phase 2 evolves to crustal rifting with effusive, flat top volcanoes with fissures; and Phase 3 is a nascent organized half-graben system with axial volcanism and seafloor spreading. The morphotectonic analysis, combined with available age constraints, shows that crustal rupture can occur rapidly (within ~1 Myr) in backarc basins but that the different rift phases can become abandoned and preserved on the seafloor as the locus of extension and magmatism migrates to focus on the ultimate zone(s) of crustal rupture. Consequently, the spatial-temporal occurrence of significant Cu-rich seafloor massive sulfide mineralization can be constrained to the transition from Phase 1 to Phase 2 within the East Manus Basin. Mineralizing hydrothermal systems have utilized interconnected structural zones developed during these phases. This research improves our understanding of the early evolution of modern backarc systems, including the association between basin evolution and spatial-temporal formation of seafloor massive sulfide deposits, and provides key morphotectonic relationships that can be used to help interpret the evolution of paleo/fossilized backarc basins found in fold belts and accreted terrains around the world.

Keywords: East Manus Basin, backarc basin, morphotectonic, basin evolution, seafloor massive sulfide deposit, Solwara 1, hydrothermal systems

OPEN ACCESS

Edited by:
Alessandro Tibaldi,
University of Milano-Bicocca, Italy

Reviewed by:
Paul Mann,
University of Houston, United States
Margaret Stewart,
Mount Royal University, Canada

****Correspondence:***
Nicholas J. Dyriw
nicholas.dyriw@qut.edu.au

Specialty section:
This article was submitted to Structural Geology and Tectonics, a section of the journal Frontiers in Earth Science

Received: *20 August 2020*
Accepted: *15 December 2020*
Published: *27 January 2021*

Citation:
Dyriw NJ, Bryan SE, Richards SW, Parianos JM, Arculus RJ and Gust DA (2021) Morphotectonic Analysis of the East Manus Basin, Papua New Guinea. Front. Earth Sci. 8:596727. doi: 10.3389/feart.2020.596727

INTRODUCTION

Modern backarc basin systems, such as the Manus and Lau, Havre, Marianas and Okinawa troughs, are important sites of extension accommodated by crustal rupture leading to new crust creation (Hannington et al., 2005; Wysoczanski et al., 2012; de Ronde et al., 2014; Monecke et al., 2014). The development of backarc basins typically occurs in rifting phases (or stages) that ultimately lead to crustal rupture followed by seafloor spreading and generation of new oceanic crust (Taylor, 1992; Clift and Leg, 1994; Parson and Wright, 1996; Fackler-Adams and Busby, 1998; Taylor and Martinez, 2003). A transition from andesite- and rhyolite-dominated, explosive volcanism and caldera-forming events during early phases of extension to mafic, effusive-style volcanism associated with flat-topped seamounts and fissures, are characteristic of many of these backarc systems (e.g., Fackler-Adams and Busby, 1998). Coupled with the compositional and volcanic transitions is the progressive development of normal faulting to organized half-graben or graben systems bounded by developing transform faults and then the establishment of spreading ridges. Established spreading ridges record complete crustal rupture and results in significant expansion in the width of the basin (e.g., Karig, 1970; Pearce et al., 1994; Taylor and Martinez, 2003; Pearce et al., 2005; Keller et al., 2008).

The spatial-temporal phase evolution of backarc systems is described for some well-studied systems such as the Lau-Havre-Taupo system (Parson and Wright, 1996; Zellmer and Taylor, 2001) and the Okinawa Trough (Sibuet et al., 1987; Sibuet et al., 1998). These studies document the spatial-temporal variations in structures, volcano morphology and geochemistry during rift evolution (see the summary in **Supplementary Table S1**). For example, a 5-phase model for the tectono-morpho-magmatic evolution of the Lau-Havre-Taupo system, in a relatively simple tectonic setting, highlights the spatial-temporal changes that are observed across the basin from initial extension through to seafloor spreading (Parson and Wright, 1996). Furthermore, a recent study on the Havre system indicates that with improved resolution, seafloor textures reveal critical information about the neovolcanic zones and sites of sediment infill in young, rapidly rifting backarc systems (Caratori Tontini et al., 2019). Improving the understanding of these systems is vital because these young systems provide a window into the processes of crustal rupture during early backarc formation (e.g., Sleeper and Martinez, 2016; Caratori Tontini et al., 2019), and these sites are also loci for significant seafloor mineralization (e.g., Wysoczanski et al., 2010; Timm et al., 2012; Wysoczanski et al., 2012; Johns et al., 2014; Monecke et al., 2014; Yeats et al., 2014).

The East Manus Basin (EMB) is the youngest and most eastward location of extensive seismicity, active volcanism, and mineralized hydrothermal activity, of the larger Manus Basin (**Figure 1**; Binns and Scott, 1993; Pegler et al., 1995; Auzende et al., 2000; Tregoning, 2002; Sinton et al., 2003; Wallace et al., 2005; Yeats et al., 2014). The EMB is also hosts the first seafloor massive sulfide (SMS) mining lease, which covers Solwara 1 Cu-Au SMS deposit (Lipton, 2012; Singer, 2014; Petersen et al., 2016). However, no morphotectonic analysis exists for the EMB. An analysis of rift evolution is important to understand because it: 1) lies at the culmination of the oblique convergence of the Australian and Pacific; 2) is influenced by subduction at the New Britain Trench (**Figure 1**; Martinez and Taylor, 1996; Taylor and Martinez, 2003; Lee and Ruellan, 2006; Baldwin et al., 2012; Holm et al., 2016); and 3) hosts some of biggest and most metal endowed seafloor massive sulfide deposits known in modern backarc terrains (Yeats et al., 2014; Petersen et al., 2016; Holm et al., 2019).

For the first time, high-resolution, datasets have been combined to undertake a comprehensive morphotectonic analysis to constrain the tectono-magmatic evolution of the EMB. This analysis provides context for understanding: 1) the early stages of backarc formation during extension; 2) spatial-temporal compositional trends and locations of magmatism within the EMB; and 3) an interpretation of how the resulting spatial and temporal framework links with the location and endowment of Cu-seafloor massive sulfide (SMS) deposit formation.

Geological Background

The Manus Basin is an active backarc basin associated with the New Britain Trench (Taylor and Martinez, 2003). The north and northeastern margins of the Manus Basin are bounded by a partly active volcanic arc, interpreted to have formed above the west-dipping subduction of the Pacific Plate (**Figure 1**; Connelly, 1976; Baldwin et al., 2012; Holm and Richards, 2013) and extends from Manus Island in the north to New Ireland in the east (Lee and Ruellan, 2006). An active, subduction-related volcanic arc bounds the southern basin margin, but the volcanism here is caused by subduction along the New Britain Trench. This volcanic arc is located above the north-dipping Solomon Plate at the New Britain Trench.

The EMB, sometimes referred to as the Southeastern Rifts, forms the easternmost extensional rift segment of the Manus Basin and covers an area of approximately 6,400 km^2 (**Figure 2**; Binns and Scott, 1993; Martinez and Taylor, 1996). Rifting within the basin is bounded to the west by the Dual Transform Fault, to the east by New Ireland and the Weitin Transform Fault (**Figure 2**; Martinez and Taylor, 1996; Lee and Ruellan, 2006; Brandl et al., 2020). The nature of crustal basement, tectonic setting and basin opening mechanisms have remained uncertain for the EMB. This is reflected in the variety of interpretations presented in past studies, including a backarc rift in old arc crust (Monecke et al., 2014); an ancient forearc crust stretched between two bounding faults in a pull-apart basin (Binns and Scott, 1993; Martinez and Taylor, 1996; Sinton et al., 2003); a transitional island arc and backarc rift (Hannington et al., 2005; Hannington et al., 2011); and a backarc spreading rift (Beaulieu et al., 2015). Microplate formation, rotation, and adjacent subduction, characterized by slab rollback of a steeply dipping slab and the formation of a slab tear add to the complexity of tectonic models of the region (Wallace et al., 2005; Baldwin et al., 2012; Holm and Richards, 2013).

The EMB began rifting ~0.78 Ma (Martinez and Taylor, 1996; Lee and Ruellan, 2006). This interpretation is based on magnetic data used for Brunhes-Matuyama polarity reversal analysis (e.g., Bassinot et al., 1994; Martinez and Taylor, 1996). Thin slithers of

TABLE 1 | Interpreted rift phase with associated volcano-tectonic characteristics. Surface characteristics presented here are similar to those observed in other well-studied extensional systems summarized in **Supplementary Table S1**.

Phase	Seafloor mode	Chemistry	Structure	Volcanic morphology	Volcanic activity
1	Remnant arc crust extension, incipient rifting (e.g., Parson and Wright, 1996)	Silicic (Patia et al., 2017)	SFD 1– relatively shallow seafloor, lack of clear normal faults, or lineations	Conical volcanoes (e.g., North Su and Nimab/Kaia Natai) caldera (Tuvai)	Unknown due to limited geophysical dataset for this area of the seafloor. Rabaul Caldera on the Gazelle Peninsula is an active volcano (Nairn et al., 1995). Tuvai caldera is silicic (Patia et al., 2017). Nimab/Kaia Natai hydrothermally active (Dekov et al., 2016)
	Current transition to nascent rifting from Phase 1 to Phase 2	Intermediate to silicic (Sinton et al., 2003; Beier et al., 2015; Thal et al., 2016; Siegburg et al., 2018)	The transition between SFD1 and SFD2. Transfer structures, steep scarps, transfer fault-oriented depressions	Conical volcano with pyroclastic deposits, shallow knolls with unknown lithofacies. Vent collapse structure of South Su. Small knoll (Suzette)	North Su – cryptodome with phreatic and phreatomagmatic explosions pyroclastic eruptive debris, blocky massive lava, plus talus (Thal et al., 2016). South Su – unknown but shows possible central vent collapse. Suzette - unknown, hyaloclastite present (Yeats et al., 2014)
2	Incipient half-graben rifting – disorganized to organized rifting which includes the development of half grabens and axial volcanic ridges (e.g., Parson and Wright, 1996). Rifting here is shallow, with widespread half grabens.	Mafic–Intermediate (Kamenetsky et al., 2001; Sinton et al., 2003; Beier et al., 2015)	SFD 2 Shallow normal faulting, transfer lineaments	Circular to irregular knolls, some with radiating fissures and some with flat tops, some small knolls. A caldera in central area	Effusive (hydroelastic) activity and fissure-fed, linear morphology
	Pual Ridge marks a transition zone	Silicic on Pual Ridge (Barriga et al., 2001; Thal et al., 2014; Beier et al., 2015)	The boundary of SFD 2 and 3	Volcanic ridge (Pual and Yuam). Point source volcanism possible on southwestern Pual Ridge, e.g., Sonne Knoll	Lobate flows (Thal et al., 2014), steep morphology
3	Developed axial half-graben rifting magmatism along the small axial ridge. Nascent organized half-graben of Kumul Ridge. Possible generation of new seafloor?	Mafic (BABB–i.e., not true ocean spreading) (Sinton et al., 2003)	SFD 3 Half-grabens developed in Kumul Ridge. > 200 m vertical throw	Oceanic ridge. symmetric spreading ridge with axial high minor small knolls developed	Axial volcanic ridge generation

positively magnetized seafloor indicate volcanism <0.78 Ma. No other absolute age constraints exist for the EMB. Rapid extension within the EMB is driven by the oblique convergence of the Pacific and Australian plates, which makes it the fastest extending section of the larger Manus Basin (Martinez and Taylor, 1996; Lindley, 2006). Furthermore, the EMB is also the locus of active, mineralized hydrothermal and volcanic centers associated with the positively magnetized seafloor, and host to Cu-rich SMS ore deposits (Binns and Scott, 1993; Binns et al., 1997; Yeats et al., 2014; Holm et al., 2016).

Convergence between the major Pacific and Australian plates and the microplate kinematics of the region influences the evolution of the Manus Basin (e.g., Martinez and Taylor, 1996; Lee and Ruellan, 2006). However, how these factors influence the EMB evolution is not clear. Part of this complexity is exacerbated because of the relative change in the convergence angle between the plates caused by NE-to EW-trending curvature of the leading plate boundary (e.g., Bird, 2003). In the southeastern corner of the EMB, the Pacific Plate converges at close to ~45°, whereas farther north along the edge of New Ireland the angle of convergence becomes less oblique and is near to sinistral strike-slip (e.g., **Figure 3**). Coupled with the effects of major plate convergence, the juxtaposed rotation of the North and South Bismarck microplates further enhance the extensional stresses on the EMB (**Figure 3**). The interactions of the opposing plate vectors invokes a transtensional stress within the EMB (Binns and Scott, 1993; Dewey et al., 1998).

A series of en-échelon volcanic edifices, associated with active hydrothermal vents, punctuate the seafloor and are built on Miocene arc crust, ranging in depth between approximately 1,200–2,750 m below sea level (Binns and Scott, 1993; Martinez and Taylor, 1996; Auzende et al., 2000; Thal et al., 2014). The seafloor massive sulfide (SMS) deposits of the EMB that are closely associated with active volcanic centers (Gamo et al., 1997; Auzende et al., 2000; Thal et al., 2014; Yeats et al., 2014) constitute some of the most copper-rich deposits of the mineral-endowed New Guinea-Solomon Islands region (Holm et al., 2019). This association is important here because the en-échelon form of the volcanoes are understood to be related to the transtensional kinematics of the EMB (Binns and Scott, 1993; Auzende et al., 2000), and therefore, may affect SMS formation. However, interpretation of the opening of the EMB suggests a

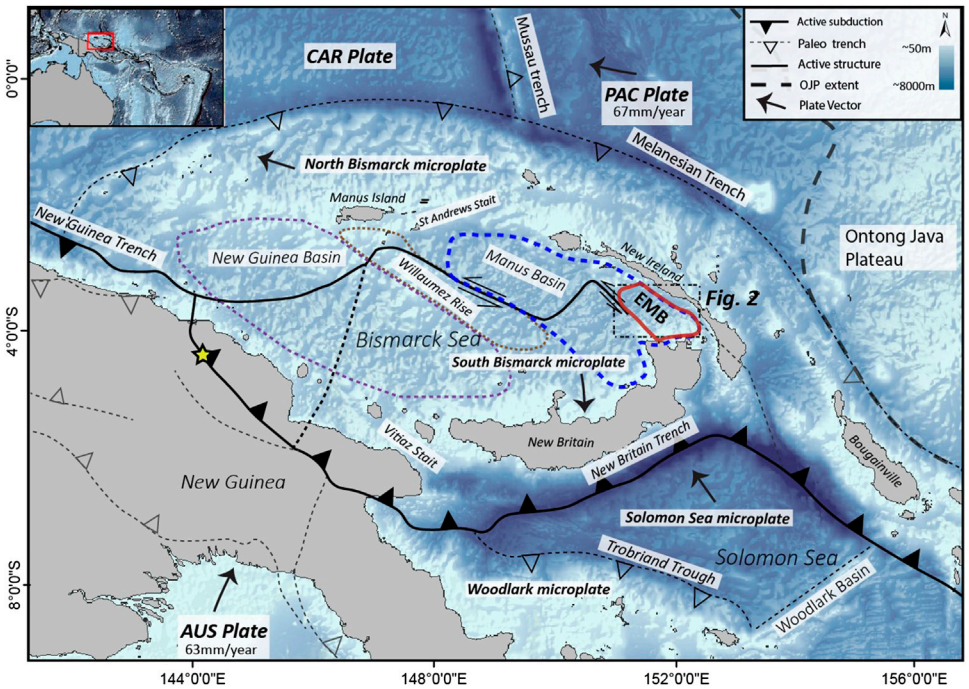

FIGURE 1 | Geological setting of the New Guinea-Solomon Islands region (After Bird, 2003; Wallace et al., 2004; Holm et al., 2016). EMB outlined in red polygon, Manus Basin outlined with blue dashed polygon, Willaumez Rise outlined with brown dashed polygon, and the New Guinea Basin outlined by purple dashed polygon. Microplate motion based on GPS vectors of the New Guinea region (Wallace et al., 2004). Yellow star indicates pole of rotation of the AUS–South Bismarck Microplates. Arrows indicate plate motion based on Euler vectors of the best fit model (Wallace et al., 2004). Bathymetry derived from General Bathymetric Chart of the Oceans (GEBCO, Weatherall et al., 2015)–IOC, IHO, and BODC, 2003, "Centenary Edition of the GEBCO Digital Atlas", Intergovernmental Oceanographic Commission and the International Hydrographic Organization as part of the General Bathymetric Chart of the Oceans; British Oceanographic Data Center, Liverpool–https://www.gebco.net/data_and_products/gridded_ bathymetry_data/gebco_30_second_grid/.

symmetric pull-apart model (e.g., Martinez and Taylor, 1996), which is not consistent with a transtensional setting. Therefore, analysis of the rift phase development is critical for the EMB to better understand the relationships between rift phase evolution and the formation of SMS deposits.

Data and Methods

This paper integrates large geophysical datasets generated by numerous research and industry exploration voyages in the EMB. A substantial regional bathymetry dataset and extensive, local, high-precision surveys provide nearly total coverage of the EMB (Barriga et al., 2001; Bach, 2011; Lipton, 2012; Yeats et al., 2014). These data, acquired from surface ships and submersible vehicles, is advantageous because bathymetric and sonic backscatter data represent the most straightforwardly observable, analyzable and interpretable expression of active tectonics. Where available, the magnetic, gravity, and seismic data also provide valuable constraints.

Bathymetric Data

Digital elevation models (DEMs) have been generated by integrating various datasets obtained by multibeam echosounder (MBES) through the EMB, covering a total area of ~6,390 km^2 (**Figure 2**). Bathymetric data collected by RV *Sonne* (expedition SO216) in 2011 (Bach, 2011), processed at 30-m pixel resolution, and various expeditions conducted by Nautilus Minerals, specifically the MV *Duke* in 2012 (Lipton, 2012), form the primary bathymetric dataset for this study. The DEMs were collated into ArcGIS software for analysis and modeling.

Surface Units and Seafloor Roughness

Seafloor acoustic backscatter, collected during MBES operations, represents the return acoustic echo reflected from the seafloor. The intensity of the return signal in the backscatter data is a qualitative but reliable measure of seafloor 'hardness' (Gonidec et al., 2003; Dartnell and Gardner, 2004). Areas of low to high reflectivity (acoustic backscatter) can be interpreted as sediment or rock outcrop, respectively. Variation in seafloor substrate type (i.e., rock or sediment), roughness (or ruggedness) and slope also affect the backscatter response. For example, fresh, smooth volcanic sheet flows with little sediment cover return a relatively strong backscatter response compared to the low reflective response of thick (>1 m) pelagic sediments.

Ideally, calibration of backscatter response to substrate lithology (e.g., volcanic rock or sediment) and grain size (e.g., Dartnell and Gardner, 2004) provides the best approach to interpret backscatter data. However, this level of detail is not available at sufficient resolution for the EMB. Backscatter interpretations for the RV *Sonne* data collected in 2011 are

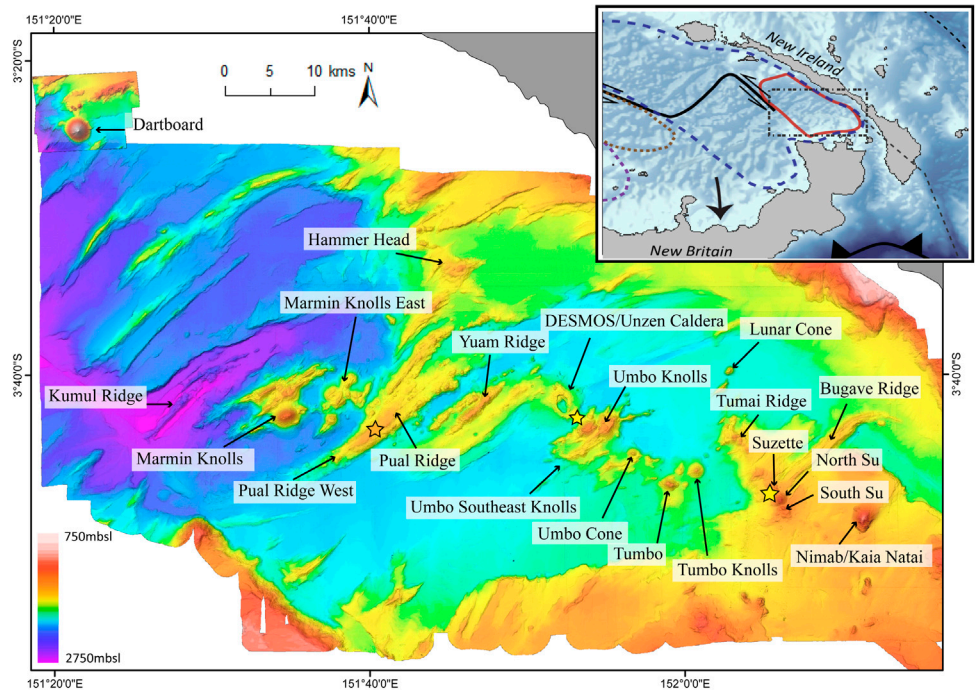

FIGURE 2 | Digital elevation model using combined bathymetric data across the EMB. RV Sonne 2011 and MV 2012 cruises are the primary bathymetric data sources. The known volcanic features are shown. Stars represent SMS systems: orange star, major mineralized hydrothermal system (e.g., PACMANUS); yellow star, Cu-Au SMS ore deposits (e.g., Solwara 1 and Solwara 12). Inset is a portion of **Figure 1** that highlights location of the EMB.

based on a combination of surface texture, slope variability and complementary ground-truth data from other studies, for example, PACMANUS (Binns and Scott, 1993; Parr and Binns, 1997; Barriga et al., 2001; Thal et al., 2014), and North Su (Binns et al., 1997; Yeats et al., 2014; Thal et al., 2016).

Interpreting backscatter data requires understanding the seafloor morphology because variations in depth, slope and roughness can return similar responses irrespective of seafloor geology. Interpretation requires continual cross-referencing with high-resolution bathymetric data to identify regions of high slope angles or variation in surface texture. For example, pillow breccias on a steep ridge may return a signal that is like volcaniclastic sediment, leading to a potential false interpretation. Visual ground-truth and sample data are not available across the entire EMB.

Sediment accumulation for the EMB is estimated at ~25 cm per 1,000 years (Binns and Scott, 1993), or about ten times higher than other backarc basins such as the Lau Basin (Gill, 1976). High terrestrial sediment input combined with volcaniclastic supply and pelagic fallout can obscure or cover features on the seafloor, leading to incorrect interpretation. Sediment distribution is important because the degree of sediment cover is typically used to estimate the age of volcanism in modern basins (e.g., Gill, 1976; Wysoczanski et al., 2010). To reduce inconsistencies in mapping and create a more reliable morphotectonic map, a sediment-outcrop interpretation was generated using the backscatter data to improve interpretation of seafloor features.

Seafloor Classification

Seafloor surface characteristics were derived from bathymetry using the Benthic Terrain Modeler (BTM) 3.0 add-on in ArcGIS v10.6 (Wright et al., 2012; Walbridge et al., 2018), and the R/V *Sonne* 2011 MBES data. The BTM is a pixel-based surface tool that allows the user to interrogate bathymetric data, on a pixel-to-pixel comparison (Walbridge et al., 2018). This tool is useful for identifying surface variation, characterizing and identifying seafloor morphology (Verfaillie et al., 2006; Rengstorf et al., 2012; Ismail et al., 2015; Watson et al., 2017; McNeil et al., 2020). This method provides a quantitative measure of seafloor variation, removing interpretation bias. Generation of the bathymetric model relies on pixel variation of the complete dataset relative to a user-defined pixel grid.

Results from the BTM raster processing includes slope, terrain ruggedness (sometimes referred to as rugosity) and aspect ratio. Slope, also referred to as the first derivative of elevation, is the maximum rate of change (elevation) within a three-by-three pixel-grid, and results are between 0° (horizontal) and 90° (vertical) across the area. Aspect ratio displays the orientation of edge faces where elevation increases relative to surrounding surfaces and helps identify and interpret orientations of lineations and faults. Terrain ruggedness generates a raster based on a ratio of the surface area of a user-defined grid normalized to a planar surface, and is a measure of the surface complexity or roughness (Du Preez, 2015). Bathymetric position index (BPI) is an analysis of the elevation of each pixel compared to the average elevation of neighboring pixels, within a user-defined neighborhood (Walbridge et al., 2018). Positive values indicate a bathymetric high such as hills,

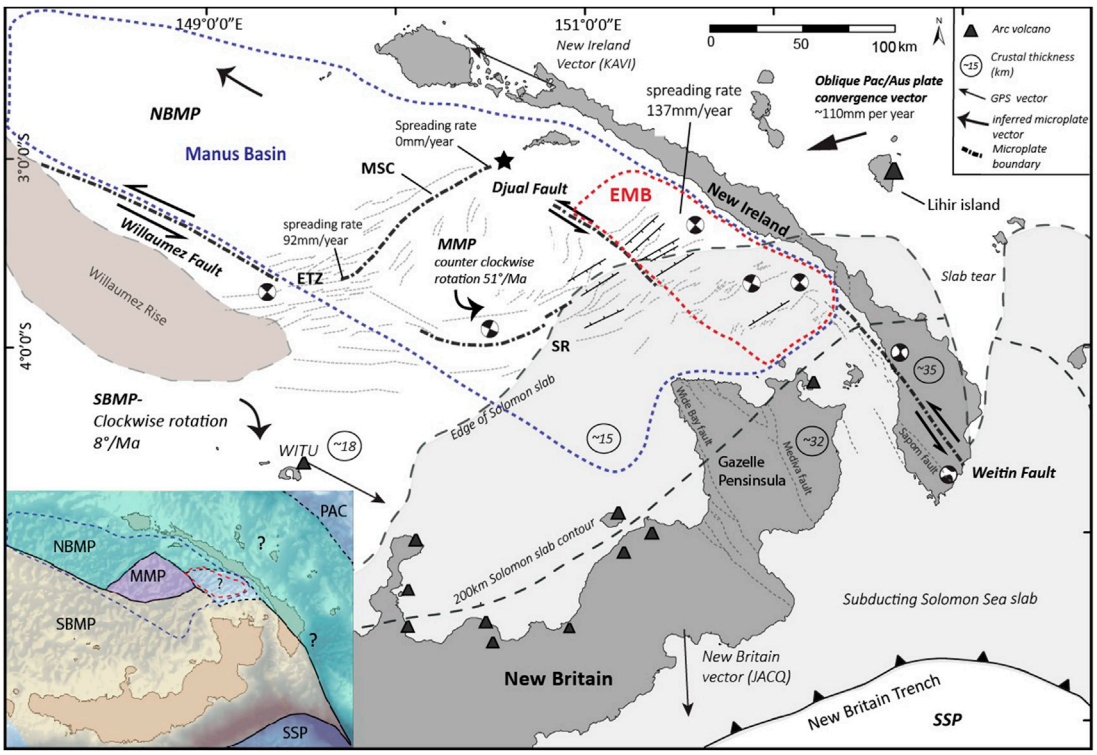

FIGURE 3 | A schematic summary of the current tectonic setting of the Manus Basin. The dashed, colored polygons highlight the extent of the Manus Basin (blue) and the EMB (red). Thick dashed black lines represent inferred microplate boundaries, that remain poorly constrained in the EMB. Abbreviations: NBMP, North Bismarck Microplate; SBMP, South Bismarck Microplate; MMP, Manus Microplate; PAC, Pacific Plate; SSP, Solomon Sea Microplate; MSC, Manus Spreading Center; ETZ, Extensional Transfer Zone; SR, Southern Rifts; EMB, East Manus Basin. WITU, KAVI, and JACQ are GPS tracking points. Black star indicates the pole of rotation for the Manus Microplate. Crustal thickness from Finlayson and Cull (1973a) and Finlayson and Cull (1973b). Focal mechanism 'beachballs' from available Harvard Centroid Moment Tensor (CMT) data (after Lee and Ruellan, 2006; Thal et al., 2014). Latest moment tensor data obtained from https://www.usgs.gov/natural-hazards/earthquake-hazards/earthquakes–accessed May 18, 2019). Major New Britain Arc volcanoes are shown as flat-topped, black triangles. Compiled data are from Taylor (1979); Taylor et al. (1994); Martinez and Taylor (1996); Tregoning et al. (1999); Tregoning et al. (2000); Tregoning (2002); Wallace et al. (2004); Wallace et al. (2005); Lee and Ruellan (2006); Lindley (2006); Wallace et al. (2009); Holm and Richards (2013); Holm et al. (2016); Lindley (2016); Thal et al. (2016). Inset shows microplates of the Manus Basin. Solid line represents known boundary, dashed line is unknown, or interpreted boundary. Uncoloured areas within the red dashed polygon indicate the unknown microplate placement in the EMB. Question marks indicate the uncertainty of the plate boundaries in the eastern area.

mounds and ridges, and negative values indicate gullies or depressions. A seafloor classification map, identifying seafloor domains, was generated from the results of these models and the classification dictionary (depth limit and slope limit columns in **Supplementary Table S2**).

Lineament identification and interpretation of seafloor structure followed common methods used in the interpretation of seafloor geophysical data. For example, first vertical derivative (1VD) magnetic data are used to "see through" sediment cover and identify lineaments at depth (e.g., Anderson et al., 2016). The term 'lineament' is used here to describe linear features that may have either structural or tectonic origins including faults and fractures, or represent linear geomorphological features such as ridge crests and volcanic chains/ridges (e.g., Peacock et al., 2016). Finally, the seafloor domain classification informed the generation of the morphotectonic map (see *Morphotectonic Map of the East Manus Basin*) through interpretation and integration of the final BTM model and DEMs with recent regional tectonic reconstructions (e.g., Martinez and Taylor, 1996; Wallace et al., 2004; Wallace et al., 2009; Holm and Richards, 2013; Holm et al., 2016).

Supplementary Geophysical Data

Limited proprietary and open-source magnetic and gravity data are available for the EMB. Manus Basin gravity and magnetic survey data collected during a 1985 research voyage of the Moana Wave, were interpreted by Martinez and Taylor (1996) and Lee and Ruellan (2006). While these data are the primary data for Manus Basin interpretation, the resolution provides only limited coverage of the EMB. These data were reprocessed (by Nautilus Minerals geophysicists) and integrated into ArcGIS for comparison and interpretation with other seafloor data. Magnetic and gravity data from some key locations complimented bathymetry for structural interpretation.

RESULTS

The BTM and bathymetry analysis are first used to identify different seafloor surface features in the EMB and then used as the foundation for the morphotectonic map. Second, the key morphotectonic features are distinguished and used to identify

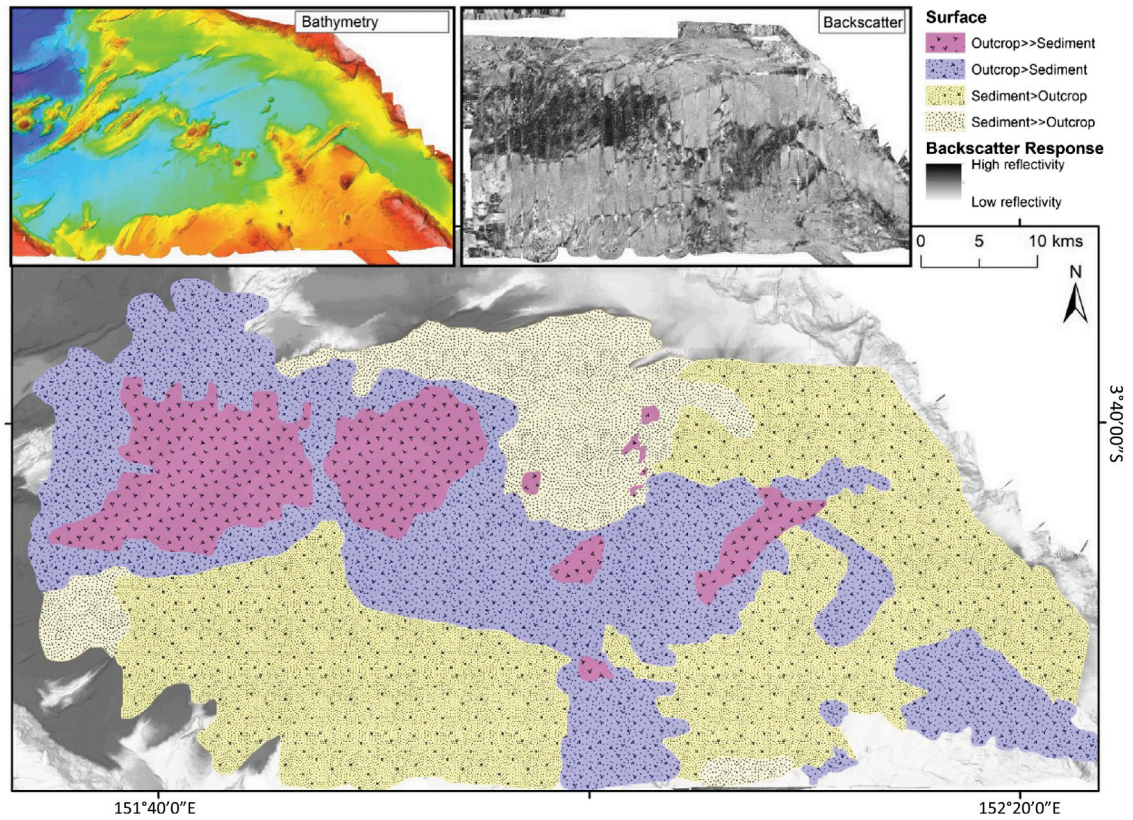

FIGURE 4 | Sediment-outcrop map of the EMB. Map polygons reflect the interpretation of surface reflectivity data. Variable sediment cover dominates. Volcanic features identified in **Figure 2** correspond to high-intensity, high-reflectivity backscatter response zones (outcrop >> sediment).

the rift phase(s), their sequence, and how these relate to other backarc systems.

Outcrop and Sediment Cover

Four different surface zones are interpreted in the EMB (**Figure 4**). These zones can be broadly grouped into: 1) sediment-dominant areas with minimal volcanic outcrop (Sediment >> Outcrop) where backscatter response is white to light gray with mottled texture; 2) Sediment-covered seafloor with sporadic volcanic outcrop (Sediment > Outcrop) where backscatter is relatively light gray and mottled; 3) exposed rock with patchy sediment cover (Outcrop > Sediment) with backscatter response showing increased darker patches within gray mottling; and, 4) volcanic outcrop-dominant with limited sediment coverage (Outcrop >> Sediment), where backscatter response is dominated by dark gray to black pixels.

Seafloor Domains of the East Manus Basin

Four geomorphic seafloor domains (SFD) of regional extent have been generated by the BTM (**Figure 5**), providing a pixel-to-pixel seafloor model, and forming the base layer for the morphotectonic map. The SFD delineate areas with varied but characteristic morphology and provide a basis for geological interpretation of rifting phases. Further details of the four SFD and their primary features are given in **Supplementary Table S2**. First-order differences in SFD are surface morphology and relative depth. Surface morphology reflects primary features (e.g., volcanic constructional features or faulting) and surface responses are affected by secondary processes (e.g., sediment cover).

SFD1 is relatively shallow (>1900 m), gently undulating and internally structureless seafloor, but is bound by rapid changes in seafloor depth (i.e., steep scarps). SFD2 and SFD 3 both occur at greater depths (2000–2,400 m) and have generally low relief, but SFD3 exhibits greater internal structuring with deep depressions bounded by steep scarps. In several cases the symmetric form to these depressions are interpreted to reflect grabens. SFD4 is separated out as a distinctive but highly varied seafloor domain characterized by abrupt and extreme changes in slope, varied roughness, variable morphology, and high backscatter intensity that often occurs within the other seafloor domains. Most of SFD4 coincides with known constructional volcanic features across the EMB (e.g., **Figure 2**), and exhibit considerable morphological complexity (**Figure 6**). The volcanic edifices assist in identifying two important basin characteristics: lithospheric-scale structures acting as pathways for ascending magmas, and the evolutionary stage of development of the EMB. Although numerous volcanoes exist in the EMB (**Figure 2**), their

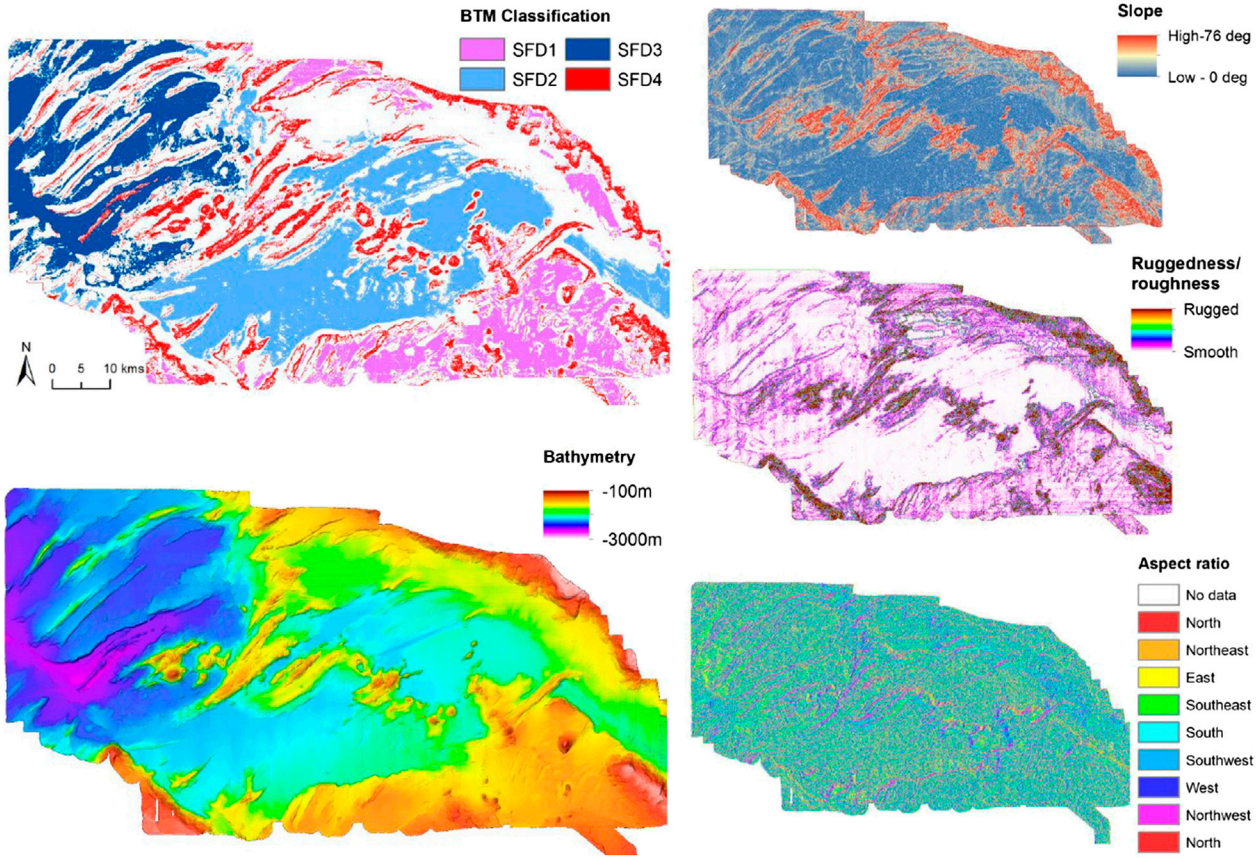

FIGURE 5 | Raster models generated from BTM classification. Pixel-based (neighborhood comparison) output from bathymetric terrain modeler. Four separate seafloor domains are identified in this classification. Included in the inset figures are bathymetric derivatives (slope, ruggedness and aspect ratio).

morphological variation across the EMB has not previously been utilized to understand rifting history.

Six volcanic morphologies are distinguished (Types 4.1–4.6) based on differences in average slope, basal extent, shape, area, relative height (relief) and backscatter response (**Figure 6**). Detailed descriptions of the volcano morphological characteristics are given in **Supplementary Table S3**. In addition to these volcano types, smaller circular features rising less than 100 m above the seafloor are identified and referred to here as mounds. Interpretation of the origins of these small-scale features is beyond the scope of this study but they reflect additional styles of seafloor volcanic eruptions from isolated vents.

Most (84%) volcanic edifices (SFD4) occur within SFD2. Apart from the Kumul Ridge within the Kumul Ridge axial rift and the Dartboard volcano (**Figure 2**), no other significant volcanic features occur to the northwest of the Kumul Rift within SFD3 (**Figure 6**). In contrast, the absence of clear constructional volcanic features within SFD3 suggests a lack of volcanism in that part of the seafloor. Of note is that the rift-parallel, elongated structures, such as the Pual Ridge (Type 4.4), are restricted to the boundaries of the SFD2 domain. Conical volcanoes like North Su (Type 4.5), are also typically found at the edges or boundaries between SFDs. DESMOS (Type 4.6), a shallow caldera structure (Gamo et al., 1997), occurs in the center of SFD2, but equivalent structures are not observed elsewhere within SFD2.

Linear Trends in the East Manus Basin

Lineaments are identified from bathymetry and complemented with magnetic first vertical derivative (1VD) data. Across the EMB, a series of northeast and northwest-trending lineaments dominate the EMB (**Figure 7**). Lineaments are readily defined from linear features in bathymetry data that exhibit a variation in seafloor depth along a continuous (linear) length. These features were cross-referenced against the aspect ratio output from BTM to ensure accurate placement. Further, where available 1VD magnetic data were used, some additional features became highlighted representing subseafloor lineaments, that are not clear from bathymetry alone. The northwest lineaments are broadly parallel to the main bounding structures and parallel to the dominant rift orientation. The northeast-trending lineaments are most well-developed in SFD3, and least developed in SFD1. In contrast, northwest-trending lineaments are delineated by a linear series of point source volcanic structures that are dominant in SFD2.

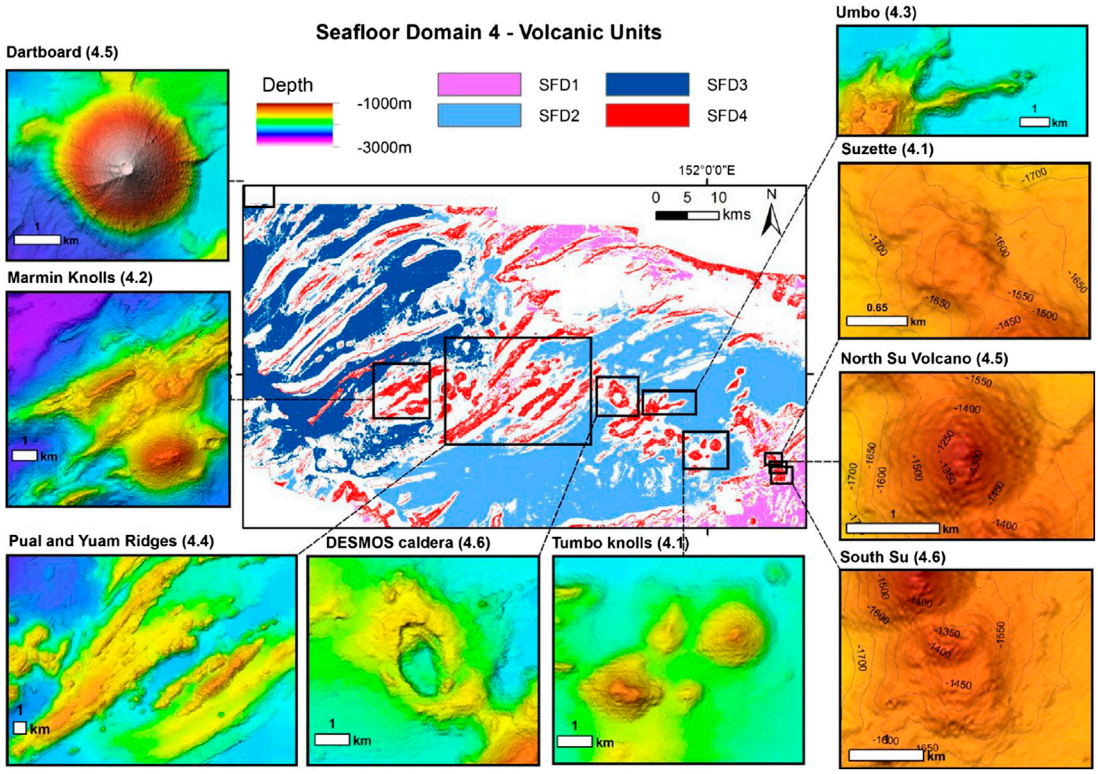

FIGURE 6 | Examples of volcanic edifices within SFD4 and their distribution across the EMB. Known and surveyed volcanic features are used here as examples with the names and Type 4 subclass shown in brackets. White scale bar for inset images represents 1 km. Base layer represents BTM results from **Figure 4**. More detailed information is given in **Supplementary Table S2**.

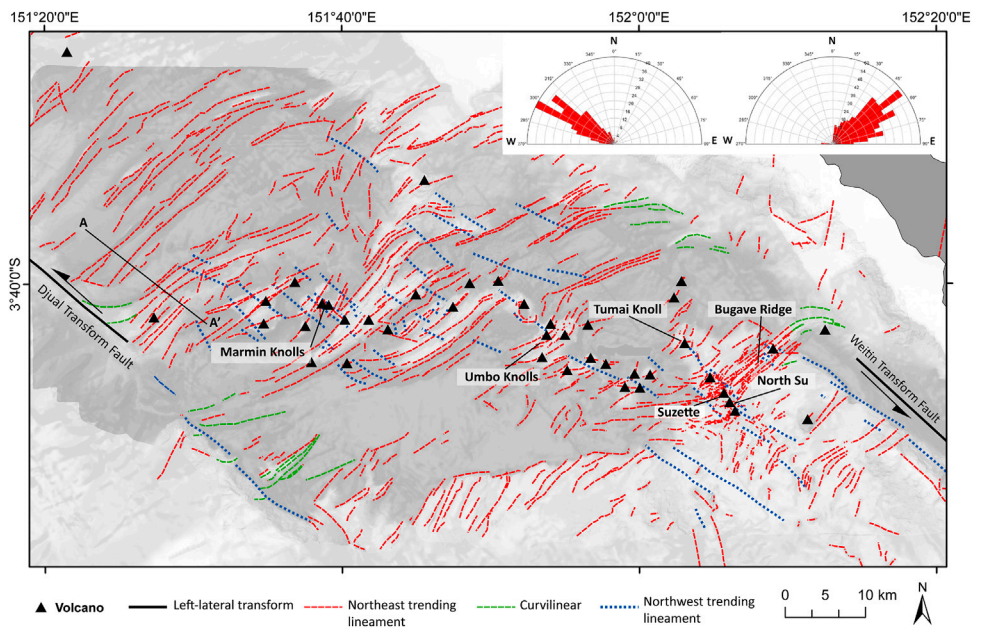

FIGURE 7 | Lineament analysis of the EMB. Lineaments are separated into four groups: left-lateral transforms (the major structures); northeast-trending; curvilinear (arcuate curved appearance); and northwest-trending. Lineament terminology is based on current structural interpretations described for the greater Manus Basin (e.g., Martinez and Taylor, 1996; Sinton et al., 2003). Black triangles identify the location of known volcanoes. Lineament orientation distribution shown in the inset.

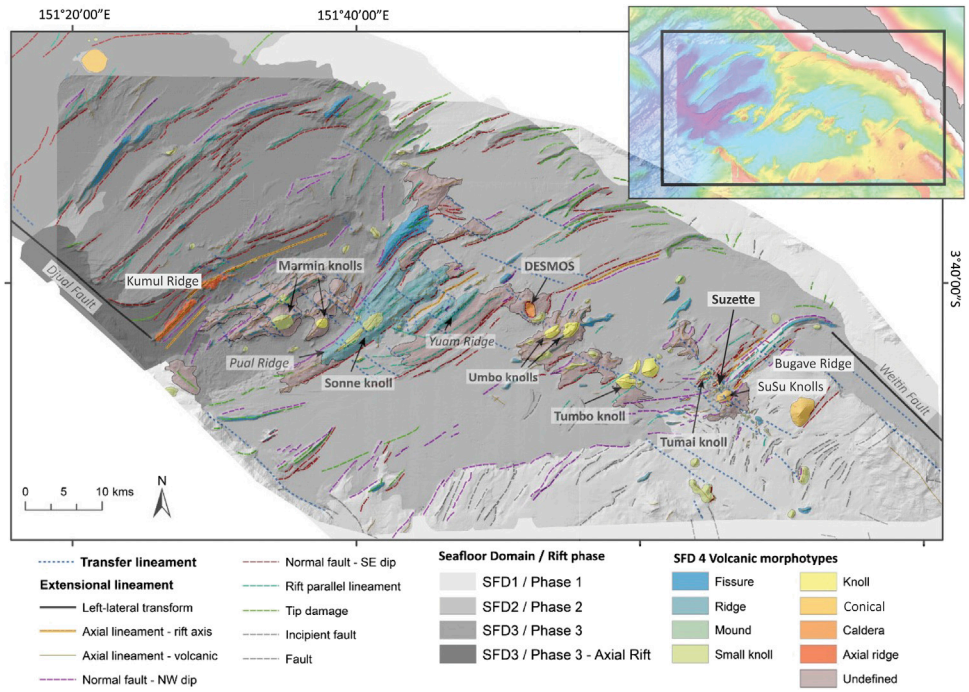

FIGURE 8 | New morphotectonic map of the EMB. Interpretation of SFD is shown in terms of rift phase. SFD4 (volcanic edifice types) are also shown and their corresponding relationship to rift phase or SFD. Lineament interpretation is also shown. Inset consists of compiled DEMs.

MORPHOTECTONIC INTERPRETATION

The four different SFDs identified for the EMB (**Figure 5**) record different expressions of extensional faulting and graben development, crustal thinning (as indicated by seafloor depth), transtension accommodation, and active volcanism. These characteristics are manifest in different stages of backarc basin evolution (e.g., Parson and Wright, 1996; Fackler-Adams and Busby, 1998; Sibuet et al., 1998; Caratori Tontini et al., 2019).

Morphotectonic Map of the East Manus Basin

The new morphotectonic map of the EMB (**Figure 8**) identifies important morphotectonic features of the EMB including: 1) lineaments and structures that control extension, transform motion, rifting and volcanism; 2) constructional, high-relief volcanic features that punctuate the seafloor and lack sedimentary cover; and 3) seafloor domains that form the basis of determining rifting phases. The map presented here shows the major morphotectonic components including prominent extensional zones, transfer lineaments and transform faults, and seafloor volcanic features associated with rifting phases within the active basin.

Lineament and Structural Terminology

We use the term "accommodation zone" to describe an area of strain between two sub-parallel, overlapping faults (Peacock et al., 2000), or soft linkages where rift boundary faults are not connected, but end and overlap (Zwaan and Schreurs, 2017). Tip damage zones represent features that develop at the terminations of transform faults and marks a jump in strain localization (Kim et al., 2004; Peacock et al., 2016).

Bounding Faults

The two primary bounding faults of the EMB are the Dual Fault in the west, and the Weitin Fault in the east (**Figure 7**). The tectonic model of Martinez and Taylor (1996) had assumed that these faults extend completely across the EMB. However, the interpretation here is that the lineation terminates at the intersection with the Kumul Ridge, where the orientation of the lineaments sharply changes from 350° to 075° (**Figure 7**). This interpretation requires that the Dual Fault terminates at the Kumul Ridge (**Figure 8**). Consequently, the stress accommodation of extension along the Dual Fault must be taken up along the Kumul Ridge. This interpretation is consistent with that of Lindley (2006) who suggested no connection exists between the submarine faults of the EMB and the major faults on the Gazelle Peninsula, eastern New Britain (**Figure 3**).

The Weitin Fault is the eastern bounding structure of the EMB (**Figure 8**; Martinez and Taylor, 1996) and is interpreted to accommodate extension in the southeastern segment within the EMB (Martinez and Taylor, 1996). A near-vertical, 200 m high scarp dips steeply toward the St Georges Channel to the east (**Figure 9**), along strike of the interpreted termination of the Weitin Fault (Finlayson and Cull, 1973a; Lee and Ruellan, 2006; Lindley, 2006). This scarp may represent the surface expression of

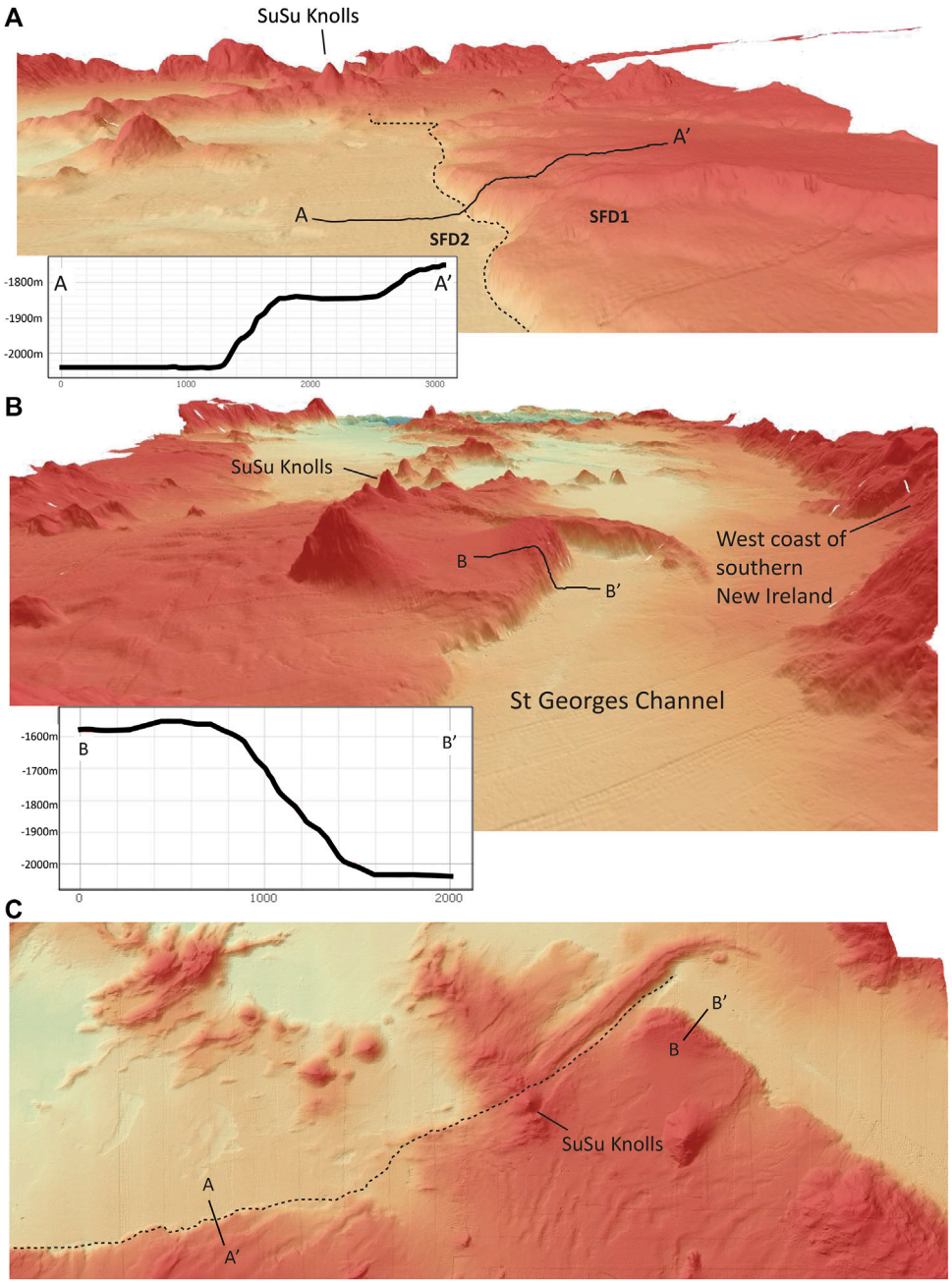

FIGURE 9 | 3D Transects across SFD 1 to SFD 2 around the SuSu Knolls area. **(A)** shows the boundary between SFD1 and SFD2 west of the SuSu Knolls, looking to the southeast. The SuSu Knolls are in the top left of the figure. Inset is a profile and highlights the steep scarp that defines the boundary. Vertical exaggeration is 2.5x. **(B)** 3D view of the St Georges Channel highlighting the fault scarp along the Weitin Fault trace. Image is 2.5x exaggerated and viewed to the northwest. Interpreted trace of the left lateral Weitin Fault lies at the base of the scarp. **(C)** Plan view showing the transects in **(A,B)**. Images and profiles were generated using QGIS (QGIS, 2016).

the steep faults of the transform fault system, consistent with previous studies that suggest the Weitin Fault is a near-vertical, large crustal-scale structure in southern New Ireland defining the boundary between the South Bismarck and Pacific plates (Lindley, 2006). However, evidence for displacement along the fault from land-based geological mapping has proved inconclusive, but the consensus is that the fault has both vertical and lateral displacement (Hohnen, 1978; Lindley, 2006). Interpretation of recent seismic activity has identified a left-lateral sense of motion at depths >10 km (moment tensor data obtained from https://www.usgs.gov/natural-hazards/earthquake-hazards/earthquakes–accessed May 18, 2019).

Previous studies showed the Weitin Fault terminating at various locations along the eastern edge the EMB. However,

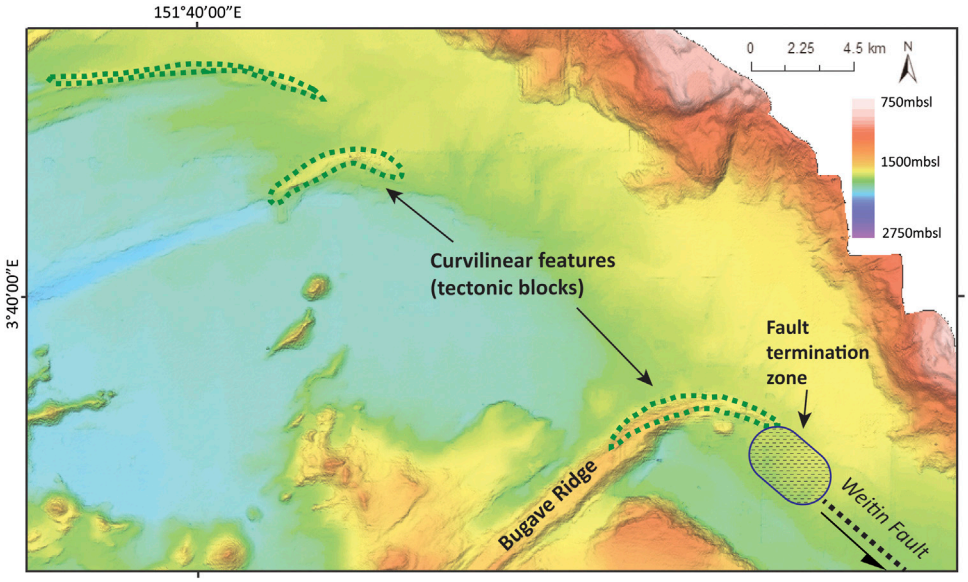

FIGURE 10 | Curvilinear features northwest of the Weitin Fault. These features are previously described by Binns and Scott (1993). An interpreted fault termination zone indicates the general location the Weitin Fault proper likely terminates.

linear structures that could relate to the extension of the Weitin Fault are not evident northwest of the Bugave Ridge (**Figure 8**). A lack of linear features may result from: 1) heavy sediment cover given this is a sediment-dominated region of the EMB (e.g., **Figure 4**); or, 2) the Weitin Fault terminating at the curved, northeastern tip of the Bugave Ridge, which is the eastern edge of SFD1 (**Figure 7**). Support for the latter scenario comes from seismic evidence that shows the locus of seismic activity does not continue north along strike of the Weitin Fault, but rather steps inboard at the Bugave Ridge across the EMB (**Supplementary Figure S1**).

Interpretation of Curvilinear Structures

A distinctive feature of SFD4 are curvilinear units that occur as bathymetric highs on the seafloor and propagate into the EMB (**Figure 10**). These elevated curvilinear structures are observed along-strike southeast and northwest of the Dual and Weitin Faults, respectively (**Figure 8**). The structures observed along-strike of the Weitin Fault, begin with the "tail" of the Bugave Ridge. These features have been described as uplifted tectonic blocks (Binns and Scott, 1993). However, the orientation, shape and placement of these features are consistent with "tip damage" zones (Kim et al., 2004). Such zones are common features of transtensional rifting regimes wherein stress, strain and slip is transferred at the termination of a transform fault (Wilson, 1965; Kim et al., 2004; Peacock et al., 2016). These structures indicate the transfer of strain toward zones of less stress and increased weakness (Kim et al., 2004). The development of these structures along-strike of the Weitin Fault likely reflects the increased strain along that edge of the EMB due to proximity of the converging Pacific Plate. The interpretation presented here proposes that these structures represent tip damage zones, which is consistent with the left-lateral shear sense of the two major faults. Accordingly, these represent the zone of strain transfer and mark the beginning of an accommodation zone in the southern part of the EMB.

More generally, structures developed between the Dual and Weitin faults are within the releasing bend of these major strike-slip structures. Releasing bends are common features in transtensional basins (Cunningham and Mann, 2007), where the movement of transform faults at the basin edges propagates across a rifting basin (e.g., Wu et al., 2009). Accordingly, there must be structures accommodating extension between the two damage zones of each transform fault within SFD 2.

Normal Faults and Half-Grabens

A series of half-graben structures, with relay ramps, dominate the deeper northwestern segment of the EMB within SFD3 (**Figure 8**). **Figure 11** is a cross-section using true surface bathymetry through the half-graben of the Kumul Ridge, with an interpretation of the subsurface structures. The lineaments are interpreted to be high-angle normal faults, with up to ~300 m of vertical relief. An axial ridge runs the length of the rift axis. The bounding faults of the half-grabens are high relief features on the seafloor that are identified in SFD4 but are not volcanic, and are distinguished by their asymmetry, smooth pixel texture and high backscatter response on the downthrown edge. Relay ramps are developed in the central and northeast regions of the half-graben sequences indicating active extension (e.g., **Figure 12**; Gawthorpe and Hurst, 1993; Peacock et al., 2016).

Normal faults are widespread across the EMB (Martinez and Taylor, 1996; Lee and Ruellan, 2006). In the absence of seismic data, linear features associated with asymmetric structures that have a down-thrown side are interpreted as normal faults. A series of linear, shallow-dipping features define the boundaries of

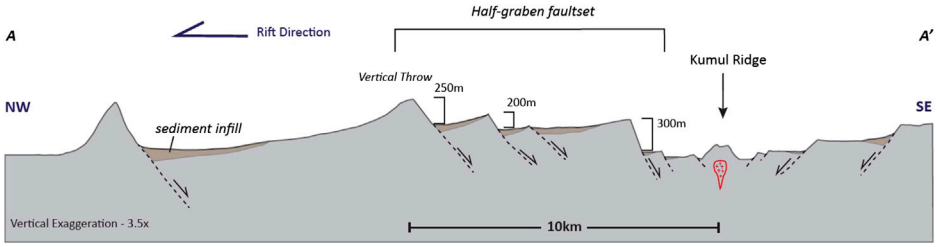

FIGURE 11 | Cross-section showing half-graben development in the northwest zone. Section line **A, A′** is shown in **Figure 6**. Sediment coverage estimated from backscatter, and seismic interpretations (Martinez and Taylor, 1996; Auzende et al., 2000; Lee and Ruellan, 2006). This half-graben feature is discussed in previous literature (e.g., Auzende et al., 2000). Extension of faults below the seafloor surface is interpreted. Sediment coverage estimated from patchy seismic data (P. Crowhurst, Nautilus Minerals, 2016, pers. comm).

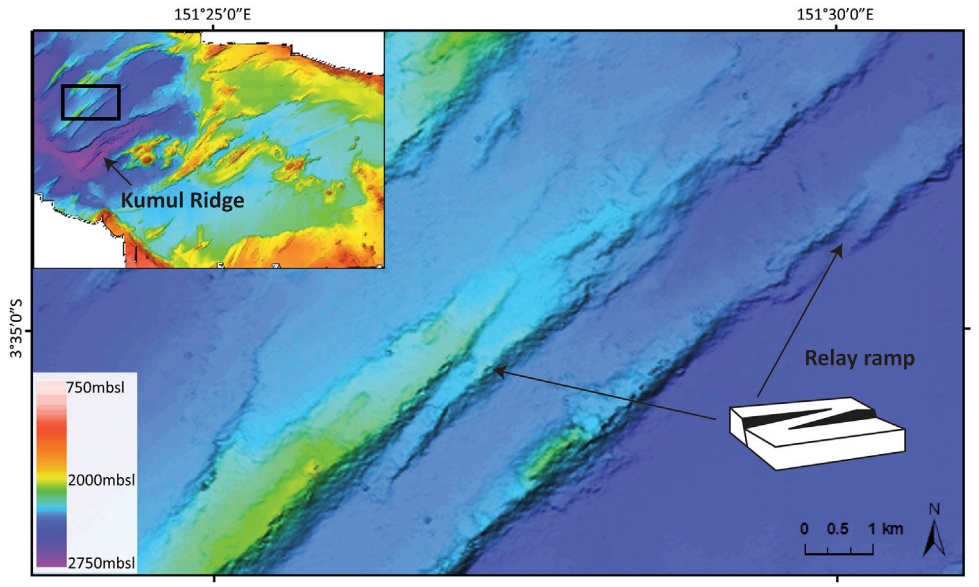

FIGURE 12 | Relay ramps within SFD3, associated with the Kumul Ridge. Relay ramp schematic after Fossen and Rotevatn (2016).

SFD2. Volcano type 4.4 (e.g., Pual Ridge), are bounded by high-angle scarps interpreted as small normal faults. High-angle scarps form the boundary between SFD 1 and 2, where subtle, linear northeast-trending depressions can be observed within the relatively shallow SFD1 (**Figure 9**). Vertical displacement varies from 100 m to 200 m, along the length of the scarp, which intersects a small cluster of northeast-trending edifices, known as the SuSu Knolls (**Figure 9**). The high-angle and displacement vector identifies the scarp as a normal fault, and is consistent with interpretations by Martinez and Taylor (1996). Farther to the northeast, the Bugave Ridge structure extends away from the SuSu Knolls and continues to the edge of the EMB, where it rotates to become a curvilinear feature (**Figure 10**).

Volcanoes and Volcanic Lineaments

The SuSu Knolls are a series of northwest-trending individual edifices that lie at the southwestern end of the Bugave Ridge, along strike of the Tumai Knoll (**Figures 7**). The SuSu Knolls, including the northern most edifice Suzette, lie at the transition between SFD1 and SFD2 (**Figure 8**). From this point north, a series of constructional volcanic edifices punctuate SFD2. The edifices are generally aligned in a northwest direction, stepping left at regular intervals across the EMB until they intersect the Yuam Ridge, the first of two elongate ridges. Ridges have an en-échelon geometry, connected to the Kumul Ridge by two knolls (Marmin Knolls) with fissures at similar orientations.

Additionally, some of the individual volcanoes, i.e., conical volcanoes and seamounts, are focused at the intersection of northwest- and northeast-trending structures (**Figure 13**). This relationship is important as these intersections may also represent zones where dilation facilitates and focuses magma and fluid migration, similar to dilational jogs proposed for some porphyry Cu ore systems (Richards et al., 2001; Richards, 2003; Sillitoe, 2010).

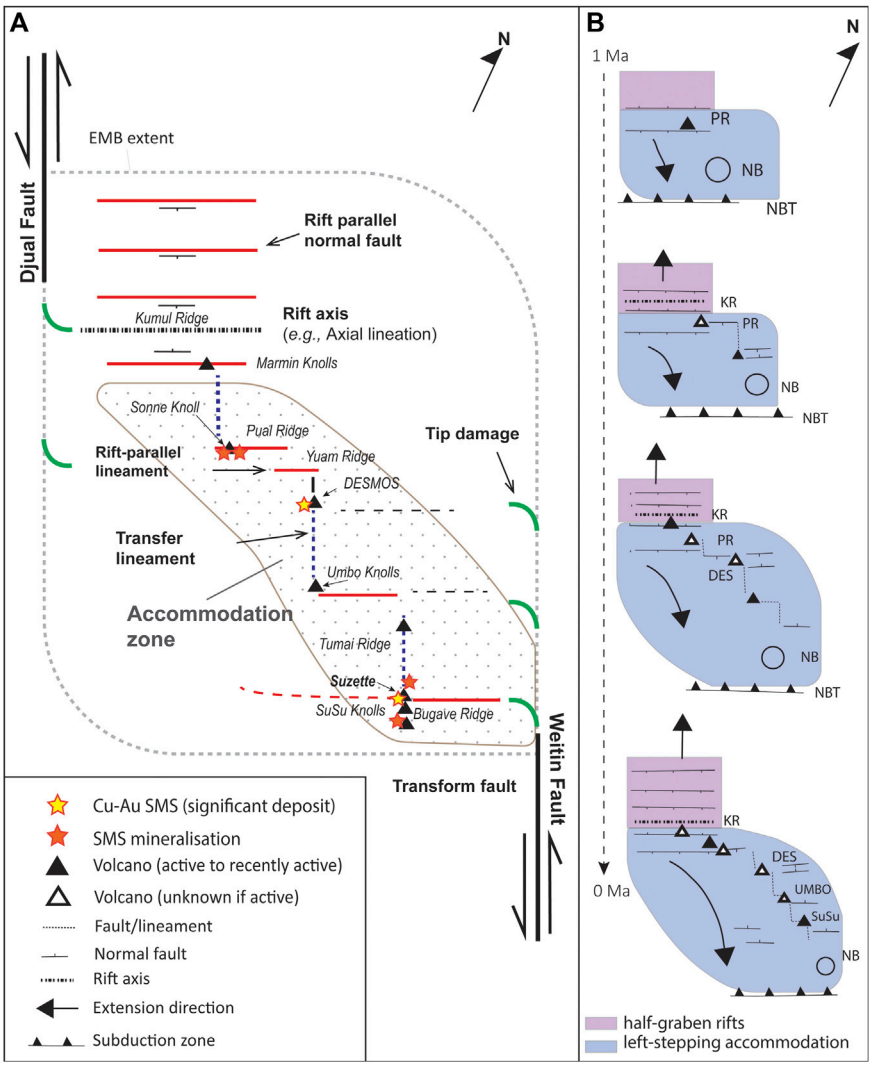

FIGURE 13 | Summary schematic showing the volcano-structural evolution of the EMB. **(A)** This simplistic schematic summarizes the variation between "classic" orthogonal rifting style in the northwest of the EMB (i.e. Kumul Ridge), and the southeast of the basin where extension is accommodated in a left-stepping accommodation zone. The more complex accommodation zone hosts the significant seafloor mineralization discovered in the EMB. Specifically, mineralization develops where cross-cutting structures intersect. Structural terms come from Gibbs (1984); Karson and Rona (1990); Mauduit and Dauteuil (1996); Kim et al. (2004); Wu et al. (2009); Peacock et al. (2016). **(B)** A schematic interpreting the ~1 Myr evolution of the EMB. Pull-apart rifting generating the half-graben rifts is interpreted to occur on the North Bismarck microplate; the left-stepping accommodation zone is interpreted to represent extension through the South Bismarck microplate. Note that the Pual Ridge and the Kumul Ridge are assumed as relatively stationary. Abbreviations: PR, Pual Ridge; KR, Kumul Ridge; DES, DESMOS, UMBO, Umbo Knolls; SuSu, SuSu Knolls (including Suzette, North and South Su); NB, New Britain (Gazelle Peninsula, identified by open circle); NBT, New Britain Trench.

The intersection of the northwest-trending SuSu Knolls (i.e., Suzette, North and South) lineament and northeast-trending Bugave Ridge is an example of this relationship. In a transtensional setting, points of crustal weakness develop along fractures and lithospheric scale structures (Wu et al., 2009). In extensional environments, locations of crustal weakness can be utilized by ascending magmas (Clift and Leg, 1994; Parson and Wright, 1996; Wright and Gamble, 1999; Wysoczanski et al., 2010). The Okinawa Trough, for example, represents an analogue of tectonic development from arc to backarc. In this system, the associated structures control volcanism within the rifted continental crust (Sibuet et al., 1987).

Volcanic features are developed along both the northwesterly and northeasterly structural trends (e.g., **Figure 7**). Linear ridges and fissures (e.g., Pual Ridge and the fissures associated with Umbo knolls) trend northeast (**Figure 8**). With overall extension in a northwest southeast direction, these features are extension-normal structures wherein magmatism is focused along fissures. Point source volcanic units, i.e., conical volcanoes, calderas and knolls/seamounts (e.g., SuSu Knolls and Umbo Knolls) occur on northwest trends. Northwest-trending series of linear clusters of individual volcanic units dominate SFD2. These volcanic lineaments are parallel with the regional bounding transform faults (i.e., the Dual and Weitin faults) but occur at the

intersection of northeast rift-parallel structures. The volcanic units do not occur as a single lineament. Instead, the volcanic lineaments are a series of left-stepping and offset to the west, where they intersect the major volcanic ridges, and the lineament terminates except for a small cluster of seamounts and fissures (e.g., Marmin Knolls) on the eastern edge of SFD 3, northwest of the Pual Ridge (**Figure 8**).

The en-échelon geometry of volcanic lineaments observed in other active submarine basins, such as the Eastern Lau Spreading Center (ESLC), has previously been suggested to be the expression of rift accommodation zones (e.g., Parson and Wright 1996). We propose these volcanic features represent magma pathways at the intersection of two structures, generated by the transtensional stress. The first tip damage structure occurs along strike of the Bugave Ridge and this marks the location of the initiation of stress transfer from the Weitin Fault inbound (i.e., to the northwest). After the termination of the Weitin Fault, the Bugave Ridge trends approximately northeast-southwest.

Similar interpretations of small, linear volcano trends defining crustal-scale structures, exist for other basins. In the NE Lau Basin for example, volcanoes are distributed along lithospheric structures that define microplate boundaries (Sleeper and Martinez, 2016); in the Havre system, linear en-échelon trends of volcanoes occur (Caratori Tontini et al., 2019). In the EMB, the en-échelon alignment (Binns and Scott, 1993) of the volcanic units and their apparent strong structural control highlights the surface expression of the major fault structures that accommodate rifting (e.g., Thal et al., 2014). The compilation of volcanic features presented here supports this hypothesis and show a systematic, linear distribution of volcanic units throughout the southeastern segments. Within SFD 2, where the volcanic units of South Su, North Su, Suzette and the Tumai Ridge occur along a northwest transect. Subsequently, a major conclusion of this interpretation is that the volcano distribution in the EMB traces the microplate boundary and Bismarck Sea Seismic Lineament.

DISCUSSION

Extension Within the East Manus Basin

A schematic interpretation of the primary lineaments and their structural importance is shown in **Figure 13**. A disparity between styles of extension accommodation exists. In the northwest, a classic pull-apart system is prevalent, with high-angle normal faults running perpendicular to a major transform fault (Dual), a linear axial ridge (Kumul Ridge), and where volcanic edifices are lacking (**Figures 5**, **7**). This morphology and interpretation conforms with the simple pull-apart model of Martinez and Taylor (1996). However in the southeast, a series of left-stepping interconnecting individual structures exist, aligned broadly in a northwest direction and in an en-échelon array (e.g., Binns and Scott, 1993). This pattern extends from the northwestern tip of the Weitin Fault to the Kumul Ridge (**Figure 13**). The disparities in styles of extension may be the result of regional kinematics: the major Pacific Plate is likely coupled with the North Bismarck microplate resulting in a northwest-directed extensional vector (e.g., Holm and Richards, 2013; Holm et al., 2016).

The South Bismarck Plate is rotating clockwise in an arcuate fashion in response to the high-angle oblique convergence between the Australian and Pacific plates, and asymmetric plate rollback at the New Britain Trench (e.g., Wallace et al., 2005; Wallace et al., 2009; Holm et al., 2016). Therefore, rather than a simple pull-apart style, extension in the southeast is accommodated by a transfer zone (**Figure 13**). In this zone, a left stepping series of rift-parallel and transform-parallel structures interconnect to accommodate extension in an arcuate pattern. Described in earlier studies as en-échelon (Binns and Scott, 1993; Martinez and Taylor, 1996; Auzende et al., 2000), it is apparent this is an accommodation zone. The accommodation zone is likely the result of extensional and strike-slip components, as the thicker crust in that area crust responds to the rapid (140 mm/year) extension driven by microplate rotation (Martinez and Taylor, 1996; Wallace et al., 2004), and the overall transtension generated by the oblique, rapid convergence of the major Australian and Pacific plates (Baldwin et al., 2012).

Basin Evolution Phases

For the larger Manus Basin, the five phases of backarc basin development (Parson and Wright, 1996) have progressed through to seafloor spreading, taking place at the Manus Spreading Center (Martinez and Taylor, 1996; Taylor and Martinez, 2003; Lee and Ruellan, 2006). However, for the EMB, three phases of backarc evolution are recognized and are specific to this extensional system. These phases comprise of: Phase 1, incipient extension; Phase 2, crustal rifting; and Phase 3, incipient seafloor spreading.

Brunhes-Matuyama polarity calculations applied to magnetic seafloor data provide the constraints to the absolute age limit to rifting in the EMB (e.g., Binns and Scott, 1993; Martinez and Taylor, 1996; Sinton et al., 2003; Lee and Ruellan, 2006). Positively magnetized seafloor in the EMB identifies zones of magmatism that are younger than the Brunhes-Matuyama polarity reversal at ~0.78 Ma (Johnson, 1982; Bassinot et al., 1994). These age limits are derived from the observation of thin slithers of 'positive' crust intersecting 'negative' pre-existing arc crust. Therefore, the associated seafloor volcanism is limited to <0.78 Ma. Sulfide mineralization at Suzette is interpreted to form from 6,000 years to present (Johns et al., 2014). The SuSu Knolls are volcanically active (Thal et al., 2016), with an eruption suspected in 2015 (Crone and Bohnenstiehl, 2019). The following rifting phases are interpreted with these age constraints.

Figure 14 illustrates the spatial extent of the three phases of basin development based on the identified seafloor domains. Despite the EMB being smaller, younger, and associated with more extreme microplate kinematics, similarities in morphotectonic characteristics between the EMB and other modern backarc basins still exist. **Table 1** summaries the features of the three phases of the EMB which are broadly similar but not identical to those listed in **Supplementary Table S1**.

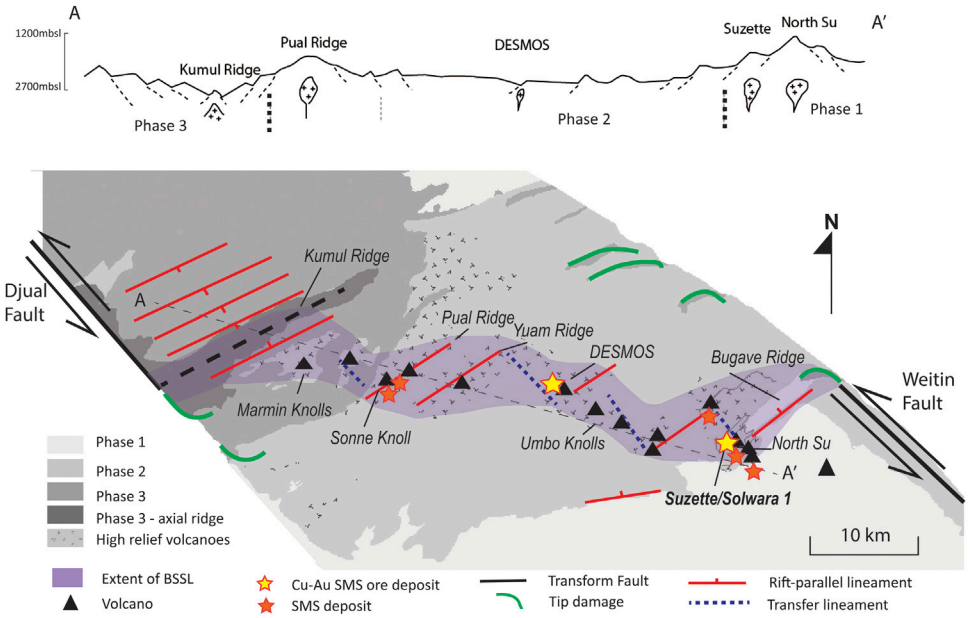

FIGURE 14 | Schematic summary of the current rift phases and trace of the of Bismarck Sea Seismic Lineament (BSSL) through the EMB. The BSSL accommodation zone is highlighted along with each rifting phase. The symbols are the same as those used in **Figure 13** for comparison. The top cross-section along the BSSL is to scale and shows interpreted normal fault traces. The stars, highlighting the SMS deposits, indicate their distribution through the EMB; the location of Solwara 1 is highlighted at the transition between Phase 1 and Phase 2, within the accommodation zone/BSSL.

We emphasize observations of the seafloor are a temporal snapshot of basin evolution. Assuming that local plate kinematics have to a first approximation remained constant, each rift phase evolves directly from the previous phase such that rifting progresses to crustal rupture and spreading center development (Karig, 1970; Parson and Wright, 1996; Caratori Tontini et al., 2019). Through this continuum, there can be some superposition of rift phases, and some areas likely preserve remnants of prior phases leading to more complexity. For example, the andesitic to dacitic Sonne Knoll, a volcanic feature on the Pual Ridge (Thal et al., 2014), may be a remnant of Phase 1 style volcanism. Although located within Phase 2 extended crust, the Sonne Knoll is compositionally similar to that of SuSu Knolls, and shares similarity in that it has a more conical style morphology yet is distinct from the surrounding rocks of the Pual Ridge (e.g., Sinton et al., 2003; Thal et al., 2014; Beier et al., 2015). More detailed analysis of the three phases of EMB evolution follows.

Phase 1–Extension of Pre-existing Arc Crust

Phase 1 is a period of incipient extension of existing arc crust (**Table 1**; **Figure 8**). SFD1 exhibits characteristic features of Phase 1 rifting, involving extension of crust coeval with poorly developed, incipient faulting. Phase 1 is characterized by:

(1) Relatively shallow (average depth ~1,670 mbsl; std. dev ~210 m) but undulating bathymetry (range = 817 to 2,149 mbsl) as represented by SFD1;
(2) A paucity of established lineaments (**Figure 7**), and seafloor structure (except at seafloor domain boundaries);
(3) Volcanic edifices that are conical volcanoes and calderas: examples include North Su, and the collapsed vent structure of the South Su volcano; and Tuvai Caldera, offshore New Britain (e.g., Patia et al., 2017).

The seafloor is relatively shallow because of the comparatively thick, preexisting arc crust (~15 km) comprising SFD1 (Finlayson and Cull, 1973b). The SFD1 domains are adjacent to the subaerial islands of New Britain and New Ireland where crustal thicknesses increase up to 32–35 km (Finlayson and Cull, 1973a; Finlayson and Cull, 1973b). Few lineaments can be identified (**Figure 7**), even in regions where little sediment cover exists (e.g., **Figure 4**). Lineament development and intensity increases toward the boundary with SFD2 domains, which is accompanied by increasing undulations of seafloor elevation.

In both modern and ancient submarine extensional basins, volcanic and structural information has been used to delineate changes in rifting phase (**Table 1**; Clift and Leg, 1994; Parson and Wright, 1996; Fackler-Adams and Busby, 1998). The characteristics of volcanic expression and erupted compositions reflect changes in rift phase such as from caldera/conical volcanoes erupting silicic magmas to fissure-fed volcanoes erupting mafic magmas (Fackler-Adams and Busby, 1998). Similar morphological transitions are evident in the EMB. Between the boundary of Phase 1 and Phase 2 seafloor, the volcanic morphology transitions from conical volcanoes, to flat top seamounts and small knolls with radiating fissures (SuSu Knolls to Umbo Knolls; **Figure 8**) Furthermore, this morphological change is concomitant with an increase in normal faulting (e.g., **Figure 8**).

Phase 2–Crustal Rifting

Phase 2 is represented by SFD2 domains, which are areas within the EMB experiencing at least the early stages of crustal rifting (**Table 1**; **Figure 8**). Key features of Phase 2 areas include:

(1) Abundant normal faults with small throws;
(2) A central constructional volcanic zone made up of knolls and flat top knolls with radiating fissures (Tumbo Knoll and Umbo Knolls) and a caldera (i.e., DESMOS);
(3) Distinctly deeper (average depth ~2055 mbsl; std. dev ~100 mbsl) and smooth seafloor (range = 1,490–2,328 mbsl), especially on the outer flanks upon which sedimentary depocenter(s) have developed.

More extended and presumably thinner crust is indicated by the depth of the seafloor, but this is not yet confirmed by geophysics (Finlayson and Cull, 1973b). Normal faults have greater along-strike continuity compared with the lineaments and faults observed across Phase 1 areas. Larger elevation changes are observed across the normal faults (up to 150 m), and where associated with volcanic ridges, the normal faults have opposing dips (northwest- and southeast-facing). These interpretations are consistent with past regional studies of the area (e.g., Martinez and Taylor, 1996; Auzende et al., 2000; Brandl et al., 2020).

Sediment cover is interpreted to dominate SFD2 as indicated by backscatter response and exceptionally smooth seafloor away from the central belt of volcanoes (**Figure. 2**). Based on the low reflectivity and smooth seafloor, we suggest shallow graben-half-graben systems across Phase 2 have been partly filled with sediment. Increased sedimentation filling fault depressions is a feature similar to those observed in the fault-bounded sediment-filled grabens of the offshore sections of the Taupo Volcanic Zone (Parson and Wright, 1996). We note the smoothest seafloor in SFD2 (**Figure 4**) is located in a similar position to the depocenters created in analogue models, which predict development of depocenters on the outer flanks of the rift within transtensional systems (e.g., Wu et al., 2009).

Volcanic features developed in Phase 2 form an approximately northwest-trending belt. Spatially, the volcano type changes from knolls and seamounts (e.g., Tumbo Knolls) at the eastern margin, to ridges and fissures in the west (e.g., Pual Ridge, Marmin Knolls; **Figure 4**). Ridges and fissures are northwest-striking, parallel to the regional extensional orientation (Martinez and Taylor, 1996). The association of more abundant northwest-striking normal faulting with volcanic ridges and fissures indicates volcanism is strongly syn-extensional in SFD2.

Of note is that the volcanic edifices and structures exhibit an offset or a series of left-steps across SFD2, (**Figure 13**–accommodation zone). The left-stepping, en-échelon nature of the volcanic edifices is interpreted to result from accommodation through this zone, and reflects the transtensional nature of rifting in this part of the EMB (e.g., **Figure 13**; Binns and Scott, 1993). This transfer zone represents the extension of the Bismarck Sea Seismic Lineament through Phase 2 (**Figure 14**).

Phase 3–Nascent Organized Half-Graben System and Axial Volcanism

Phase three represents seafloor areas within the EMB that have experienced more protracted rifting and crustal thinning, as exemplified by SFD3. It is similar to Phase 3 of Parson and Wright, 1996 (**Table 1**). The Pual Ridge (**Figure 8**) marks the boundary between Phase 2 and Phase 3 and the corresponding SFD. Phase 3 is characterized by:

(1) Deeper seafloor (average ~2,330 mbsl; std. dev ~200 mbsl);
(2) A set of mid-to high-angle, south-dipping, inward-facing, normal faults, part of half-graben structures, and relay ramp;
(3) A linear axial volcanic ridge; and
(4) A lack of volcanism to the northwest of the axial ridge.

A well-developed half-graben sequence is observed along the Dual Fault (**Figure 11**). The half-grabens are ~30 km wide and can be traced for ~20 km along strike. A set of relay ramps observed to the northwest of the axial ridge confirm a kinematic linkage of normal faults (**Figure 12**). Backscatter response confirms the half grabens are sediment-filled. Similar half-graben systems have been described from the Ngatoroirangi Rift, Southern Havre Trough (Wysoczanski et al., 2010), and the evolution of the western and eastern Havre Trough (e.g., Caratori Tontini et al., 2019). The lack of constructional volcanoes in this area is consistent with observations from the Rumble and Ngatoro rifts in the southern Havre Trough (Parson and Wright, 1996). We conclude extensional tectonism is recorded by SFD3 and it shares morphological, structural, and volcanic similarities with Phase 3 of Parson and Wright (1996).

The elevated axial ridge and a flanking graben structure at the Kumul Ridge are features indicative of recent volcanism and nascent seafloor spreading (e.g., **Figure 11**; Parr and Binns, 1997). These features are consistent with those described and observed in other rifts in the Southwest Pacific. For example, the Ngatoroirangi Rift in the Havre Trough exhibits a similar axial valley high, produced by pillow and lobate flows, within the broad graben (Wysoczanski et al., 2010). Furthermore, dominant fault scarps extending 20–30 km sub-parallel to the axial ridge, with throws of ~200–250 m are features of fast-spreading ridges (Carbotte and Macdonald, 1994). It is unlikely the Kumul Ridge has produced large volumes of lava, based on seafloor magnetization and Brunhes-Matuyama results from the SeaMARC survey (Martinez and Taylor, 1996), and the small extent of the axial ridge in the bathymetric data. Seismic evidence suggests the axial trace may still be active.

We propose that the Kumul Ridge is not currently a true oceanic spreading center given the absence of a seafloor magnetic signature as observed for the Manus Spreading Center (**Figure 3**; Martinez and Taylor, 1996). The muted magnetic response over the Kumul Ridge indicates limited magmatism has occurred over the last one Myr (Martinez and Taylor, 1996; Lee and Ruellan, 2006). Furthermore, the axial ridge is a half-graben rift developed normal to the Dual transform fault. Compositions from a limited number of basaltic samples collected by CSIRO from the Kumul Ridge have a backarc basin signature (eg, higher large ion

lithophile elements, SiO_2, Al_2O_3 and H_2O; and low FeO^*, TiO_2, and CaO, and are light rare earth element enriched compared to MORB). These rocks are also geochemically distinct compared to other samples collected further to the southeast from DESMOS to Bugave Ridge, which exhibit a progressively increasing arc-like geochemical signature (Sinton et al., 2003; Park et al., 2010).

Bismarck Sea Seismic Lineament

Defining the extension of the Bismarck Sea Seismic Lineament (BSSL) into the EMB is crucial to understanding the development of rifting and volcanism. The BSSL is the plate boundary between the microplates of the Bismarck Sea: the North Bismarck, South Bismarck and Manus Microplates (**Figure 3**; Martinez and Taylor, 1996). To date, extension of the BSSL into the EMB has not been well documented. **Figure 14** illustrates schematically the spatial distribution of the rift phases and identifies the possible trace of the BSSL. This interpreted trace of the BSSL is consistent with an active, shallow (<50 km) zone of seismicity coincident with volcanic features at the surface (**Supplementary Figure S1**). We propose the BSSL extends into the EMB at the termination of the Dual Fault, along the Kumul Ridge, and broadly tracks the location of volcanic features at surface (**Figure 14**). This interpretation is based on the termination of the transfer faults, occurrence of tip damage zone, and the density and spatial distribution of the shallow (<20 km) earthquakes.

Rifting Models for the East Manus Basin

The kinematic and structural model of Martinez and Taylor (1996) for the EMB outlines a symmetric, pull-apart basin setting. Two bounding transform faults are a requirement of this model to accommodate the observed extension and rifting, and to develop a symmetrical pull-apart basin. In a young, modern rifting system, these transform faults should be evident at the surface as dominant linear features, such as in the Gulf of California (Lonsdale, 1989; Ferrari et al., 2013). We identify two aspects of this model that require modification given the data presented here: 1) basin symmetry and seafloor expression of the bounding transform faults; and 2) the development of half-graben systems.

The western edge of the Weitin Fault lacks seafloor morphological features that are characteristic of half-graben sequences (**Figure 8**). The scarp along the edge of the Weitin Fault marks the edge of SFD1, and the relatively shallower, gently undulating seafloor of SFD1 generally lacks evidence of well-developed normal faults like those north of the Kumul Ridge in SFD3 (**Figure 8**). The extent and distribution of the different SFD across the EMB also lack symmetry. Therefore, considering that the seafloor varies markedly in the northern and southern sections, a revised interpretation of the EMB rifting phases is needed.

Archetypal active back-arc basins such as the Lau-Havre Trough system (Karig, 1970; Parson and Wright, 1996; Caratori Tontini et al., 2019) and Marianas (Martinez and Taylor, 2003; Stern et al., 2003; Pearce et al., 2005) have developed along long convergent plate boundaries with long histories of continuous subduction between large tectonic plates (e.g., Australia-Pacific). In the EMB, the rifting environment is more complex and is due to the combination of:

(1) Rapid microplate rotation (Tregoning et al., 2000; Tregoning, 2002; Wallace et al., 2005);
(2) The oblique and rapid convergence of the Pacific and Australian plates (Baldwin et al., 2012);
(3) Plate coupling between the North Bismarck Microplate and the Pacific Plate (Martinez and Taylor, 1996);
(4) Relatively thick, pre-existing arc crust (Finlayson and Cull, 1973a; Finlayson and Cull, 1973b);
(5) Deep and steep subduction (Holm and Richards, 2013);
(6) Oblique slab rollback (Holm et al., 2016); and
(7) A plate tear on the subducting Solomon Sea slab (Holm and Richards, 2013).

Extension in the EMB has been ongoing over the last ~1 Myr (Martinez and Taylor, 1996; Kamenetsky et al., 2001). Seafloor characteristics observed in the EMB highlight the diversity of features generated in the earliest stages in the transition from an arc to backarc basin: varied bathymetry and volcano morphology exist in these transitional terrains. Therefore, the associated characteristics observed in the EMB should be used as a guide for observation of other modern systems in very early stages of arc to backarc transition rather than for a direct comparison with more mature backarc basin systems.

Implications for Mineralization in the East Manus Basin

This study now places the known SMS deposits of the EMB in a morphotectonic context. An improved tectono-magmatic understanding is critical for the deposits in the EMB, because recent studies of mineralization suggest direct magmatic involvement in the formation of these deposits, both in the EMB (Yang and Scott, 2002; 2005; Yeats et al., 2014; Dekov et al., 2016) and in other arc-backarc systems in the Southwest Pacific (de Ronde et al., 2005; Wysoczanski et al., 2012; Li et al., 2016). Significant SMS are associated with point source volcanoes at the intersection of the northwest- and northeast-trending structures. This relationship is best illustrated at the intersection of the Bugave Ridge and the SuSu Knolls (**Figure 13**). The Suzette edifice lies directly on top of this intersection and hosts the Solwara 1 Cu-SMS ore deposit (Lipton, 2012; Yeats et al., 2014). Most other SMS deposits in the EMB are associated with edifices at these intersections and are restricted to SFD1 and SFD2.

We propose the morphotectonic setting in the EMB is significant in terms of localization of mineralization. This relationship is observed for magmatic-hydrothermal systems in other settings such as those of porphyry Cu deposits in tectonically complex crustal settings. For example, the combination of oblique plate convergence at crustal boundaries (Richards, 2009), subduction and structural intersections that generate dilational zones (Wu et al., 2009; Piquer et al., 2016) are critical for Cu-Au ore deposit formation (e.g., Escondido and Chuquicamata, Chile

(Richards et al., 2001; Sillitoe, 2010; Hervé et al., 2012; Rivera et al., 2012). Identifying, and exploring for these structures are common practice employed in porphyry Cu–Au and epithermal exploration (Glen and Walshe, 1999; Richards, 2003; Sillitoe, 2010; Glen, 2013). Furthermore, observations from some Australian VMS terrains propose that primary syn-volcanic faults are important in ore-focusing, but are generally hard to distinguish (Large, 1992). As demonstrated here, a relationship exists between volcanism and cross-cutting rift-parallel and rift-oblique structures, and these components are intimately linked to mineralized SMS systems (e.g., **Figures 13**, **14**).

A critical interpretation here is the accommodation zone acts as a releasing bend within the extending crust in the EMB. We propose that this fault network develops dilational conduits, where magma and fluid can migrate and undergo focused flow to the surface. This structural setting may account for the disparity of known SMS north of the Pual Ridge, where simple pull-apart rifting dominates, and lacks these dilational conduits. Evidence from the morphotectonic framework presented here suggests syn-volcanic faults are directly related to focusing magmatic activity and ore-generating fluids in early rifting arc to back arc terrains.

CONCLUSION

The compilation of open source and proprietary industry geophysical data has culminated in the first morphotectonic map of the EMB (**Figure 8**). The geomorphometric analysis provided a technique to assess the nature of rifting in the EMB, in the general absence of seismic data. Seafloor modeling of bathymetric data using the BTM software identified four distinct seafloor domains. A series of structural and volcano-morphological features associated with each phase presents an opportunity to examine the relationship between the phases of basin development, structures, volcanism, and associated mineralization. Within each phase, the basin-bounding faults and volcanism reflect a complex but non-unique set of features that develop in different seafloor domains during the evolution from an arc to backarc environment.

The EMB exhibits three phases of rifting from 'early extension of pre-existing crust' to 'nascent seafloor spreading'. Phase 1 represents the early extension of pre-existing arc crust, and particularly characterizes the southern margin of the EMB. The high-angle fault scarp along the northern edge of Phase 1, and the linear series of volcanic units (the SuSu Knolls), spatially mark the transition of Phase 1 to Phase 2. This sharp transition is important because it signals a change to more organized rift structures and has spatial-temporal context to mineralization. Rift-parallel ridges (Pual and Yuam) mark the transition between Phase 2 and Phase 3. An organized half-graben system exemplifies Phase 3 rifting. In the deepest locations, rifting has evolved to form a ridge high and marks the transition to nascent seafloor spreading.

The pre-existing crust is progressively thinned from Phase 1 to Phase 3. The presence of half-graben structures in Phase 3 suggest that the crust there has undergone more extension than in Phase 1. Half-graben structures are not present in Phase 1 because the thicker crust that underlies those regions has undergone limited extension. The variation in seafloor characteristics are also a consequence of the plate kinematics. Specifically, the orientation of the convergence of the Pacific Plate into the southern half of the EMB is at a lower angle than in the north (e.g., Hall, 2002; Bird, 2003). Using these regional kinematic indicators is critical for the local scale interpretation of rifting within the EMB. Major plate convergence combined with the juxtaposed rotation of the microplates results in a greater transtensional stress in the southern half of the EMB. It is the interaction of these macro-to microplate kinematics that leads to the varied extension and accommodation styles in the EMB.

Two principal structural components are interpreted to control rifting. The first is a northeast-trending, rift-parallel structural fabric that accommodates extension. The second is a series of northwest-trending volcanic-defined lineaments that represent accommodation zones, which transfer the stress associated with the oblique convergence of the Pacific and Bismarck microplates plates, particularly across Phase 1 and Phase 2.

The observations and interpretations here suggest that primary structural intersections are important for modern extensional magmatic-hydrothermal provinces, like the EMB. These structural intersections form dilational features along fault bends that may act as conduits for magma and fluid migration. Within the EMB, significant Cu mineralization occurs at the intersection of northwest-and northeast-trending structures. Solwara 1 Cu-Au SMS deposit is located at the intersection of the rift-parallel Bugave Ridge and the transfer-parallel SuSu Knolls volcanic lineament. This association indicates that economic Cu mineralization may be intimately linked to these intersecting structures and the transition between early rifting Phases 1 and 2.

DATA AVAILABILITY STATEMENT

The data analyzed in this study is subject to the following licenses/restrictions: Contact the corresponding author to access bathymetric data. Requests to access these datasets should be directed to nicholas.dyriw@qut.edu.au.

AUTHOR CONTRIBUTIONS

NJD wrote the first draft of the manuscript, originally as part of a chapter of his PhD thesis. NJD developed and in collaboration with SWR and JMP refined the tectonic story. All authors contributed to the manuscript revision, read, and approved the submitted version.

FUNDING

This work is from NJD PhD research project in which he was supported by a RTP PhD scholarship. Manuscript preparation was also supported by a QUT Write-up scholarship, supported by DAG. Nautilus Minerals provided in-kind funding in the form of free access to geophysical data sets.

ACKNOWLEDGMENTS

We wish to acknowledge Dr. Wolfgang Bach for permitting the use of the Sonne dataset and Captain and crew of the Sonne 2011 expedition for their work in collecting excellent geophysical data. We further thank Wolfgang Bach and Janis Thal for their discussions regarding the Sonne 2011 dataset. We also wish to acknowledge the crew of the Duke 2012 their work in collecting further high-quality geophysical data. We acknowledge the developers of the Benthic Terrain Modeler software for ArcGIS. ND also acknowledges the extended conversations with Sean Plunkett and Peter Crowhurst (formerly Nautilus Minerals) in developing early thoughts and refining ideas of the tectonic development of the EMB. Sean Plunkett (formerly Nautilus Minerals) is thanked for the initial processing of MBES and other geophysical data, and discussions around the evolution of the EMB. Lastly, we extend our thanks to the two reviewers, and the editor, for robust and constructive feedback.

SUPPLEMENTARY MATERIAL

The Supplementary Material for this article can be found online at: https://www.frontiersin.org/articles/10.3389/feart.2020.596727/full#supplementary-material.

REFERENCES

Anderson, M. O., Hannington, M. D., Haase, K., Schwarz-Schampera, U., Augustin, N., McConachy, T. F., et al. (2016). Tectonic focusing of voluminous basaltic eruptions in magma-deficient backarc rifts. *Earth Planet Sci. Lett.* 440, 43–55. doi:10.1016/j.epsl.2016.02.002

Auzende, J.-M., Ishibashi, J.-I., Beaudoin, Y., Charlou, J.-L., Delteil, J., Donval, J.-P., et al. (2000). Extensive magmatic and hydrothermal activity documented in manus basin. *Eos Trans. Am. Geophys. Union.* 81 (39), 449–453. doi:10.1029/00eo00331

Bach, W. (2011). Report and preliminary results of RV SONNE Cruise SO 216, Townsville (Australia)-Makassar (Indonesia), June 14 July 23, 2011. BAMBUS, Back-Arc Manus Basin Underwater Solfataras. *Berichte, Fachbereich Geowissenschaften, Universität Bremen*. Available at: https://media.suub.uni-bremen.de/bitstream/elib/2914/1/00102250-1.pdf (Accessed January 23, 2019).

Baldwin, S. L., Fitzgerald, P. G., and Webb, L. E. (2012). Tectonics of the new Guinea region. *Annu. Rev. Earth Planet Sci.* 40, 495–520. doi:10.1146/annurev-earth-040809-152540

Barriga, F. J. A. S., Binns, R. A., and Party, S. S. (2001). Leg 193 preliminary report: anatomy of an active felsic-hosted hydrothermal system, eastern manus basin. *Ocean Drill. Program.* 193, 1–71. doi:10.2973/odp.proc.sr.193.201.2007

Bassinot, F. C., Labeyrie, L. D., Vincent, E., Quidelleur, X., Shackleton, N. J., and Lancelot, Y. (1994). The astronomical theory of climate and the age of the Brunhes-Matuyama magnetic reversal. *Earth Planet Sci. Lett.* 126 (1-3), 91–108

Beaulieu, S. E., Baker, E. T., and German, C. R. (2015). Where are the undiscovered hydrothermal vents on oceanic spreading ridges?. *Deep Sea Res. Part II Top. Stud. Oceanogr.* 121, 202–212. doi:10.1016/j.dsr2.2015.05.001

Beier, C., Bach, W., Turner, S., Niedermeier, D., Woodhead, J., Erzinger, J., et al. (2015). Origin of silicic magmas at spreading centres—an example from the south east rift, manus basin. *J. Petrol.* 56 (2), 255–272. doi:10.1093/petrology/egu077

Binns, R. A., and Scott, S. D. (1993). Actively forming polymetallic sulfide deposits associated with felsic volcanic rocks in the eastern manus back-arc basin, papua new guinea. *Econ. Geol.* 88 (8), 2226–2236. doi:10.2113/gsecongeo.88.8.2226

Binns, R., Scott, S., Gemmell, J., and Crook, K. (1997). Shipboard Party, 1997, the Susu knolls hydrothermal field, eastern Manus basin, Papua New Guinea [abs.]. *Eos.* 78 (46), F772

Bird, P. (2003). An updated digital model of plate boundaries. *G-cubed.* 4 (3), 1027. doi:10.1029/2001GC000252

Brandl, P. A., Hannington, M. D., Geersen, J., Petersen, S., and Gennerich, H.-H. (2020). The submarine tectono-magmatic framework of Cu-Au endowment in the Tabar-to-Feni island chain, PNG. *Ore Geol. Rev.* 121, 103491. doi:10.1016/j.oregeorev.2020.103491

Caratori Tontini, F., Bassett, D., de Ronde, C. E. J., Timm, C., and Wysoczanski, R. (2019). Early evolution of a young back-arc basin in the havre trough. *Nat. Geosci.* 12 (10), 856–862. doi:10.1038/s41561-019-0439-y

Carbotte, S. M., and Macdonald, K. C. (1994). Comparison of seafloor tectonic fabric at intermediate, fast, and super fast spreading ridges: influence of spreading rate, plate motions, and ridge segmentation on fault patterns. *J. Geophys. Res. Solid Earth.* 99 (B7), 13609–13631

Clift, P. D., and Leg, O. (1994). Volcanism and sedimentation in a rifting island-arc terrain: an example from tonga, SW pacific. *Geol. Soc. London Spec. Publ.* 81 (1), 29–51

Connelly, J. (1976). Tectonic development of the bismarck Sea based on gravity and magnetic modelling. *Geophys. J. Int.* 46 (1), 23–40

Crone, T. J., and Bohnenstiehl, D. R. (2019). Acoustic evidence of a long-lived gas-driven submarine volcanic eruption in the bismarck sea. *Geophys. J. Int.* 217 (1), 169–178. doi:10.1093/gji/ggy542

Cunningham, W., and Mann, P. (2007). Tectonics of strike-slip restraining and releasing bends. *Geol. Soc. London Spec. Publ.* 290 (1), 1–12. doi:10.1144/sp290.1

Dartnell, P., and Gardner, J. V. (2004). Predicting seafloor facies from multibeam bathymetry and backscatter data. *Photogramm. Eng. Rem. Sens.* 70 (9), 1081–1091. doi:10.14358/pers.70.9.1081

de Ronde, C. E. J., Hannington, M. D., Stoffers, P., Wright, I. C., Ditchburn, R. G., Reyes, A. G., et al. (2005). Evolution of a submarine magmatic-hydrothermal system: brothers volcano, southern kermadec arc, new zealand. *Econ. Geol.* 100 (6), 1097–1133. doi:10.2113/gsecongeo.100.6.1097%J Economic Geology

de Ronde, C. E. J., Hein, J. R., and Butterfield, D. A. (2014). Metallogenesis and mineralization of intraoceanic arcs II: the aeolian, izu-bonin, mariana, and kermadec arcs, and the manus backarc basin—introduction. *Econ. Geol.* 109 (8), 2073–2077. doi:10.2113/econgeo.109.8.2073

Dekov, V. M., Rouxel, O., Kouzmanov, K., Bindi, L., Asael, D., Fouquet, Y., et al. (2016). Enargite-luzonite hydrothermal vents in manus back-arc basin: submarine analogues of high-sulfidation epithermal mineralization. *Chem. Geol.* 438, 36–57. doi:10.1016/j.chemgeo.2016.05.021

Dewey, J., Holdsworth, R., and Strachan, R. (1998). Transpression and transtension zones. *Geol. Soc. London Spec. Publ.* 135 (1), 1–14

Du Preez, C. (2015). A new arc–chord ratio (ACR) rugosity index for quantifying three-dimensional landscape structural complexity. *Landsc. Ecol.* 30 (1), 181–192. doi:10.1007/s10980-014-0118-8

Fackler-Adams, B. N., and Busby, C. J. (1998). Structural and stratigraphic evolution of extensional oceanic arcs. *Geology.* 26 (8), 735–738

Ferrari, L., López-Martínez, M., Orozco-Esquivel, T., Bryan, S. E., Duque-Trujillo, J., Lonsdale, P., et al. (2013). Late oligocene to middle Miocene rifting and synextensional magmatism in the southwestern sierra madre Occidental, Mexico: the beginning of the Gulf of California rift. *Geosphere.* 9 (5), 1161–1200. doi:10.1130/GES00925.1

Finlayson, D., and Cull, J. (1973a). Structural profiles in the new britain/new Ireland region. *J. Geol. Soc. Aust.* 20 (1), 37–47

Finlayson, D., and Cull, J. (1973b). Time-term analysis of new britain-new Ireland island arc structures. *Geophys. J. Int.* 33 (3), 265–280

Fossen, H., and Rotevatn, A. (2016). Fault linkage and relay structures in extensional settings—a review. *Earth Sci. Rev.* 154, 14–28. doi:10.1016/j.earscirev.2015.11.014

Gamo, T., Okamura, K., Charlou, J.-L., Urabe, T., Auzende, J.-M., Ishibashi, J., et al. (1997). Acidic and sulfate-rich hydrothermal fluids from the Manus back-arc basin, Papua New Guinea. *Geology.* 25 (2), 139–142. doi:10.1130/0091-7613(1997)025<0139:aasrhf>2.3.co.2

Gawthorpe, R., and Hurst, J. M. (1993). Transfer zones in extensional basins: their structural style and influence on drainage development and stratigraphy. *J. Geol. Soc.* 150 (6), 1137–1152

Gibbs, A. D. (1984). Structural evolution of extensional basin margins. *J. Geol. Soc.* 141 (4), 609–620. doi:10.1144/gsjgs.141.4.0609

Gill, J. B. (1976). Composition and age of Lau Basin and Ridge volcanic rocks: implications for evolution of an interarc basin and remnant arc. *GSA Bulletin.* 87, 1384–1395. doi:10.1130/0016-7606(1976)87<1384CAAOLB>2.0.CO

Glen, R. (2013). Refining accretionary orogen models for the Tasmanides of eastern Australia. *Aust. J. Earth Sci.* 60 (3), 315–370. doi:10.1080/08120099.2013.772537

Glen, R., and Walshe, J. (1999). Cross-structures in the lachlan orogen: the lachlan transverse zone example. *Aust. J. Earth Sci.* 46 (4), 641–658

Gonidec, Y. L., Lamarche, G., and Wright, I. C. (2003). Inhomogeneous substrate analysis using EM300 backscatter imagery. *Mar. Geophys. Res.* 24 (3), 311–327. doi:10.1007/s11001-004-1945-9

Hall, R. (2002). Cenozoic geological and plate tectonic evolution of SE Asia and the SW Pacific: computer-based reconstructions, model and animations. *J. Asian Earth Sci.* 20 (4), 353–431. doi:10.1016/s1367-9120(01)00069-4

Hannington, M. D., de Ronde, C. D., and Petersen, S. (2005). Sea-floor tectonics and submarine hydrothermal systems. *Econ. Geol.* 100, 111–114. doi:10.5382/av100.06

Hannington, M., Jamieson, J., Monecke, T., Petersen, S., and Beaulieu, S. (2011). The abundance of seafloor massive sulfide deposits. *Geology.* 39 (12), 1155–1158. doi:10.1130/g32468.1

Hervé, M., Sillitoe, R., Wong, C., Fernández, P., Crignola, F., Ipinza, M., et al. (2012). Geologic overview of the Escondido porphyry copper district, northern Chile. *Soc. Econ. Geol. Spec. Publ.* 16, 55–78. doi:10.5382/SP.16.03

Hohnen, P. (1978). Geology of new Ireland, Papua New Guinea. *BMR Bulletin.* 194, 39

Holm, R. J., and Richards, S. W. (2013). A re-evaluation of arc–continent collision and along-arc variation in the Bismarck Sea region, Papua New Guinea. *Aust. J. Earth Sci.* 60 (5), 605–619. doi:10.1080/08120099.2013.824505

Holm, R. J., Rosenbaum, G., and Richards, S. W. (2016). Post 8 Ma reconstruction of Papua New Guinea and Solomon Islands: microplate tectonics in a convergent plate boundary setting. *Earth Sci. Rev.* 156, 66–81. doi:10.1016/j.earscirev.2016.03.005

Holm, R. J., Tapster, S., Jelsma, H. A., Rosenbaum, G., and Mark, D. F. (2019). Tectonic evolution and copper-gold metallogenesis of the Papua New Guinea and Solomon Islands region. *Ore Geol. Rev.* 104, 208–226. doi:10.1016/j.oregeorev.2018.11.007

Ismail, K., Huvenne, V. A. I., and Masson, D. G. (2015). Objective automated classification technique for marine landscape mapping in submarine canyons. *Mar. Geol.* 362 (Suppl. C), 17–32. doi:10.1016/j.margeo.2015.01.006

Johns, S. M., Ditchburn, R. G., Barry, B. J., and Yeats, C. J. (2014). Episodic subseafloor hydrothermal activity within the eastern Manus back-arc basin determined by uranium-series disequilibrium in barite. *Econ. Geol.* 109 (8), 2227–2242. doi:10.2113/econgeo.109.8.2227

Johnson, R. (1982). Brunhes-Matuyama magnetic reversal dated at 790,000 yr BP by marine-astronomical correlations. *Quat. Res.* 17 (2), 135–147

Kamenetsky, V. S., Binns, R. A., Gemmell, J. B., Crawford, A. J., Mernagh, T. P., Maas, R., et al. (2001). Parental basaltic melts and fluids in eastern Manus backarc Basin: implications for hydrothermal mineralisation. *Earth Planet Sci. Lett.* 184 (3–4), 685–702. doi:10.1016/S0012-821X(00)00352-6

Karig, D. E. (1970). Ridges and basins of the Tonga-Kermadec island arc system. *J. Geophys. Res.* 75 (2), 239–254

Karson, J. A., and Rona, P. A. (1990). Block-tilting, transfer faults, and structural control of magmatic and hydrothermal processes the TAG area, Mid-Atlantic Ridge 26° N. *Geol. Soc. Am. Bull.* 102 (12), 1635–1645

Keller, N. S., Arculus, R. J., Hermann, J., and Richards, S. (2008). Submarine back-arc lava with arc signature: fonualei spreading center, northeast Lau Basin, Tonga. *J. Geophys. Res.: Solid Earth.* 113 (B8), B08S07. doi:10.1029/2007JB005451

Kim, Y.-S., Peacock, D. C. P., and Sanderson, D. J. (2004). Fault damage zones. *J. Struct. Geol.* 26 (3), 503–517. doi:10.1016/j.jsg.2003.08.002

Large, R. R. (1992). Australian volcanic-hosted massive sulfide deposits; features, styles, and genetic models. *Econ. Geol.* 87 (3), 471–510. doi:10.2113/gsecongeo.87.3.471

Lee, S.-M., and Ruellan, E. (2006). "Tectonic and magmatic evolution of the Bismarck Sea, Papua New Guinea: review and new synthesis," in *Back-arc spreading systems: geological, biological, chemical, and physical interactions.* Editor D. M. Christie (Washington, DC: American Geophysical Union), 263–286.

Li, Z. G., Chu, F. Y., Dong, Y. H., Li, X. H., Liu, J. Q., Yang, K. H., et al. (2016). Origin of selective enrichment of Cu and Au in sulfide deposits formed at immature back-arc ridges: examples from the Lau and Manus basins. *Ore Geol. Rev.* 74, 52–62. doi:10.1016/j.oregeorev.2015.11.010

Lindley, I. D. (2006). *Extensional and vertical tectonics in the New Guinea islands: implications for island arc evolution.* Editors G. Lavecchia and G. Scalera Rome, Italy, 403–426.

Lindley, I. D. (2016). Plate flexure and volcanism: late cenozoic tectonics of the tabar–lihir–tanga–feni alkalic province, new Ireland basin, Papua New Guinea. *Tectonophysics.* 677-678 (Suppl. C), 312–323. doi:10.1016/j.tecto.2016.04.015

Lipton, I. (2012). *Mineral resources estimate–solwara project bismarck sea, PNG. Golder Associates Pty Ltd. Golder Resource Report, 107631040-003.*

Lonsdale, P. (1989). *Geology and tectonic history of the Gulf of California.* The Eastern Pacific Ocean and Hawaii. Boulder, CO: Geological Society of America, Geology of North America, v. N, 499–521.

Martinez, F., and Taylor, B. (1996). Backarc spreading, rifting, and microplate rotation, between transform faults in the Manus Basin. *Mar. Geophys. Res.* 18 (2), 203–224

Martinez, F., and Taylor, B. (2003). Controls on back-arc crustal accretion: insights from the Lau, Manus and Mariana basins. *Geol. Soc. London Spec. Publ.* 219 (1), 19–54.

Mauduit, T., and Dauteuil, O. (1996). Small-scale models of oceanic transform zones. *J. Geophys. Res. Solid Earth.* 101 (B9), 20195–20209. doi:10.1029/96JB01509

McNeil, M. A., Nothdurft, L. D., Dyriw, N. J., Webster, J. M., and Beaman, R. J. (2020). Morphotype differentiation in the Great Barrier Reef Halimeda bioherm carbonate factory: internal architecture and surface geomorphometrics. *Depositional Record.* [Epub ahead of print]. doi:10.1002/dep2.122

Monecke, T., Petersen, S., and Hannington, M. D. (2014). Constraints on water depth of massive sulfide formation: evidence from modern seafloor hydrothermal systems in Arc-related settings. *Econ. Geol.* 109 (8), 2079–2101. doi:10.2113/econgeo.109.8.2079

Nairn, I. A., McKee, C. O., Talai, B., and Wood, C. P. (1995). Geology and eruptive history of the Rabaul Caldera area, Papua New Guinea. *J. Volcanol. Geoth. Res.* 69 (3), 255–284. doi:10.1016/0377-0273(95)00035-6

Park, S.-H., Lee, S.-M., Kamenov, G. D., Kwon, S.-T., and Lee, K.-Y. (2010). Tracing the origin of subduction components beneath the south east Rift in the Manus Basin, Papua New Guinea. *Chem. Geol.* 269 (3–4), 339–349. doi:10.1016/j.chemgeo.2009.10.008

Parr, J. M., and Binns, R. A. (1997). *Exploration and mining report 345R - report on the PACMANUS-III cruise.* Papua New Guinea: RV Franklin, Eastern Manus BasinCSIRO.

Parson, L. M., and Wright, I. C. (1996). The Lau-Havre-Taupo back-arc basin: a southward-propagating, multi-stage evolution from rifting to spreading. *Tectonophysics.* 263 (1), 1–22. doi:10.1016/S0040-1951(96)00029-7

Patia, H., Eggins, S. M., Arculus, R. J., McKee, C. O., Johnson, R. W., and Bradney, A. (2017). The 1994–2001 eruptive period at Rabaul, Papua New Guinea: petrological and geochemical evidence for basalt injections into a shallow dacite magma reservoir, and significant SO2 flux. *J. Volcanol. Geoth. Res.* 345, 200–217. doi:10.1016/j.jvolgeores.2017.08.011

Peacock, D. C. P., Knipe, R. J., and Sanderson, D. J. (2000). Glossary of normal faults. *J. Struct. Geol.* 22 (3), 291–305. doi:10.1016/S0191-8141(00)80102-9

Peacock, D. C. P., Nixon, C. W., Rotevatn, A., Sanderson, D. J., and Zuluaga, L. F. (2016). Glossary of fault and other fracture networks. *J. Struct. Geol.* 92, 12–29. doi:10.1016/j.jsg.2016.09.008

Pearce, J. A., Ernewein, M., Bloomer, S. H., Parson, L. M., Murton, B. J., and Johnson, L. E. (1994). Geochemistry of Lau Basin volcanic rocks: influence of ridge segmentation and arc proximity. *Geol. Soc. London Spec. Publ.* 81 (1), 53–75

Pearce, J. A., Stern, R. J., Bloomer, S. H., and Fryer, P. (2005). Geochemical mapping of the Mariana arc-basin system: implications for the nature and distribution of subduction components. *Geochem. Geophys. Geosyst.* 6 (7), Q07006. doi:10.1029/2004GC000895

Pegler, G., Das, S., and Woodhouse, J. (1995). A seismological study of the eastern New Guinea and the western Solomon Sea regions and its tectonic implications. *Geophys. J. Int.* 122 (3), 961–981

Petersen, S., Krätschell, A., Augustin, N., Jamieson, J., Hein, J. R., and Hannington, M. D. (2016). News from the seabed – geological characteristics and resource potential of deep-sea mineral resources. *Mar. Pol.* 70, 175–187. doi:10.1016/j.marpol.2016.03.012

Piquer, J., Berry, R. F., Scott, R. J., and Cooke, D. R. (2016). Arc-oblique fault systems: their role in the Cenozoic structural evolution and metallogenesis of the Andes of central Chile. *J. Struct. Geol.* 89, 101–117. doi:10.1016/j.jsg.2016.05.008

QGIS (2016). *QGIS geographic information system.*: Open source geospatial foundation project

Rengstorf, A. M., Grehan, A., Yesson, C., and Brown, C. (2012). Towards high-resolution habitat suitability modeling of vulnerable marine ecosystems in the deep-sea: resolving terrain attribute dependencies. *Mar. Geodes.* 35 (4), 343–361. doi:10.1080/01490419.2012.699020

Richards, J. P., Boyce, A. J., and Pringle, M. S. (2001). Geologic evolution of the Escondido area, northern Chile: a model for spatial and temporal localization of porphyry Cu mineralization. *Econ. Geol.* 96 (2), 271–305. doi:10.2113/gsecongeo.96.2.271

Richards, J. P. (2009). Postsubduction porphyry Cu-Au and epithermal Au deposits: products of remelting of subduction-modified lithosphere. *Geology.* 37 (3), 247–250. doi:10.1130/g25451a.1

Richards, J. P. (2003). Tectona-magmatic precursors for porphyry Cu-(Mo-Au) deposit formation. *Econ. Geol.* 98 (8), 1515–1533. doi:10.2113/gsecongeo.98.8.1515

Rivera, S., Alcota, H., Proffett, J., Díaz, J., Leiva, G., and Vergara, M. (2012). Update of the geologic setting and porphyry Cu-Mo deposits of the Chuquicamata district, northern Chile. *Soc. Econ. Geol.* 16, 19–54. doi:10.5382/sp.16.02

Sibuet, J. C., Deffontaines, B., Hsu, S. K., Thareau, N., Formal, L., and Liu, C. S. (1998). Okinawa trough backarc basin: early tectonic and magmatic evolution. *J. Geophys. Res. Solid Earth.* 103 (B12), 30245–30267

Sibuet, J. C., Letouzey, J., Barbier, F., Charvet, J., Foucher, J. P., Hilde, T. W., et al. (1987). back arc extension in the Okinawa trough. *J. Geophys. Res. Solid Earth.* 92 (B13), 14041–14063

Siegburg, M., Klügel, A., Rocholl, A., and Bach, W. (2018). Magma plumbing and hybrid magma formation at an active back-arc basin volcano: north Su, eastern Manus basin. *J. Volcanol. Geoth. Res.* 362, 1–16. doi:10.1016/j.jvolgeores.2018.07.001

Sillitoe, R. H. (2010). Porphyry copper systems. *Econ. Geol.* 105 (1), 3–41. doi:10.2113/gsecongeo.105.1.3

Singer, D. A. (2014). Base and precious metal resources in seafloor massive sulfide deposits. *Ore Geol. Rev.* 59 (0), 66–72. doi:10.1016/j.oregeorev.2013.11.008

Sinton, J. M., Ford, L. l., Chappell, B., and Mcculloch, M. T. (2003). Magma genesis and mantle heterogeneity in the Manus back-arc basin, Papua New Guinea. *J. Petrol.* 44 (1), 159–195. doi:10.1093/petrology/44.1.159

Sleeper, J. D., and Martinez, F. (2016). Geology and kinematics of the Niuafo'ou microplate in the northern Lau Basin. *J. Geophys. Res. Solid Earth.* 121 (7), 4852–4875. doi:10.1002/2016jb013051

Stern, R. J., Fouch, M. J., and Klemperer, S. L. (2003). An overview of the Izu-Bonin-Mariana subduction factory. inside subduction factory. *Geophys. Monogr. Ser.* 138, 175–222. doi:10.1029/138gm10

Taylor, B. (1979). Bismarck Sea: evolution of a back-arc basin. *Geology.* 7 (4), 171–174. doi:1130/0091-7613

Taylor, B., Crook, K., and Sinton, J. (1994). Extensional transform zones and oblique spreading centers. *J. Geophys. Res. Solid Earth.* 99 (B10), 19707–19718. doi:10.1029/94JB01662

Taylor, B., and Martinez, F. (2003). Back-arc basin basalt systematics. *Earth Planet Sci. Lett.* 210 (3-4), 481–497. doi:10.1016/s0012-821x(03)00167-5

Taylor, B. (1992). "Rifting and the volcanic-tectonic evolution of the Izu-Bonin-Mariana arc," in Proceedings of Ocean Drilling Program (College Station, TX, USA: Scientific Results), Vol. 126, 625–651.

Thal, J., Tivey, M., Yoerger, D., Jöns, N., and Bach, W. (2014). Geologic setting of PACManus hydrothermal area–high resolution mapping and *in situ* observations. *Mar. Geol.* 355 (0), 98–114. doi:10.1016/j.margeo.2014.05.011

Thal, J., Tivey, M., Yoerger, D. R., and Bach, W. (2016). Subaqueous cryptodome eruption, hydrothermal activity and related seafloor morphologies on the andesitic North Su volcano. *J. Volcanol. Geoth. Res.* 323, 80–96. doi:10.1016/j.jvolgeores.2016.04.041

Timm, C., de Ronde, C. E. J., Leybourne, M. I., Layton-Matthews, D., and Graham, I. J. (2012). Sources of chalcophile and siderophile elements in kermadec arc lavas*. *Econ. Geol.* 107 (8), 1527–1538. doi:10.2113/econgeo.107.8.1527

Tregoning, P., Jackson, R. J., McQueen, H., Lambeck, K., Stevens, C., Little, R. P., et al. (1999). Motion of the south Bismarck Plate, Papua New Guinea. *Geophys. Res. Lett.* 26 (23), 3517–3520

Tregoning, P., McQueen, H., Lambeck, K., Jackson, R., Little, R., Saunders, S., et al. (2000). Present-day crustal motion in Papua New Guinea. *Earth Planets Space.* 52 (10), 727–730. doi:10.1186/BF03352272

Tregoning, P. (2002). Plate kinematics in the western Pacific derived from geodetic observations. *J. Geophys. Res. Solid Earth.* 107 (B1), ECV 7–1–ECV 7–8. doi:10.1029/2001JB000406

Verfaillie, E., Van Lancker, V., and Van Meirvenne, M. (2006). Multivariate geostatistics for the predictive modelling of the surficial sand distribution in shelf seas. *Continent. Shelf Res.* 26 (19), 2454–2468. doi:10.1016/j.csr.2006.07.028

Walbridge, S., Slocum, N., Pobuda, M., and Wright, D. (2018). Unified geomorphological analysis workflows with benthic terrain modeler. *Geosciences.* 8 (3), 94. doi:10.3390/geosciences8030094

Wallace, L. M., Ellis, S., and Mann, P. (2009). Collisional model for rapid fore-arc block rotations, arc curvature, and episodic back-arc rifting in subduction settings. *Geochem. Geophys. Geosyst.* 10 (5), Q05001. doi:10.1029/2008GC002220

Wallace, L. M., McCaffrey, R., Beavan, J., and Ellis, S. (2005). Rapid microplate rotations and backarc rifting at the transition between collision and subduction. *Geology.* 33 (11), 857–860. doi:10.1130/g21834.1

Wallace, L. M., Stevens, C., Silver, E., McCaffrey, R., Loratung, W., Hasiata, S., et al. (2004). GPS and seismological constraints on active tectonics and arc-continent collision in Papua New Guinea: implications for mechanics of microplate rotations in a plate boundary zone. *J. Geophys. Res. Solid Earth.* 109 (B5), B05404. doi:10.1029/2003JB002481

Watson, S. J., Whittaker, J. M., Lucieer, V., Coffin, M. F., and Lamarche, G. (2017). Erosional and depositional processes on the submarine flanks of Ontong Java and Nukumanu atolls, western equatorial Pacific Ocean. *Mar. Geol.* 392 (Suppl. C), 122–139. doi:10.1016/j.margeo.2017.08.006

Weatherall, P., Marks, K. M., Jakobsson, M., Schmitt, T., Tani, S., Arndt, J. E., et al. (2015). A new digital bathymetric model of the world's oceans. *Earth Space Sci.* 2 (8), 331–345. doi:10.1002/2015EA000107

Wilson, J. T. (1965). Transform faults, oceanic ridges, and magnetic anomalies southwest of vancouver island. *Science.* 150 (3695), 482–485. doi:10.1126/science.150.3695.482

Wright, D., Pendleton, M., Boulware, J., Walbridge, S., Gerlt, B., Eslinger, D., et al. (2012). *ArcGIS benthic terrain modeler (BTM), v. 3.0.*. Corvallis, OR: Environmental Systems Research Institute, NOAA Coastal Services Center, Massachusetts Office of Coastal Zone Management.

Wright, I. C., and Gamble, J. A. (1999). Southern Kermadec submarine caldera arc volcanoes (SW Pacific): caldera formation by effusive and pyroclastic eruption. *Mar. Geol.* 161 (2–4), 207–227. doi:10.1016/S0025-3227(99)00040-7

Wu, J. E., McClay, K., Whitehouse, P., and Dooley, T. (2009). 4D analogue modelling of transtensional pull-apart basins. *Mar. Petrol. Geol.* 26 (8), 1608–1623. doi:10.1016/j.marpetgeo.2008.06.007

Wysoczanski, R. J., Handler, M. R., Schipper, C. I., Leybourne, M. I., Creech, J., Rotella, M. D., et al. (2012). The tectonomagmatic source of ore metals and volatile elements in the southern kermadec arc. *Econ. Geol.* 107 (8), 1539–1556. doi:10.2113/econgeo.107.8.1539

Wysoczanski, R., Todd, E., Wright, I., Leybourne, M., Hergt, J., Adam, C., et al. (2010). Backarc rifting, constructional volcanism and nascent disorganised spreading in the southern Havre Trough backarc rifts (SW Pacific). *J. Volcanol. Geoth. Res.* 190 (1), 39–57. doi:10.1016/j.jvolgeores.2009.04.004

Yang, K., and Scott, S. D. (2002). Magmatic degassing of volatiles and ore metals into a hydrothermal system on the modern sea floor of the eastern Manus back-arc basin, western pacific. *Econ. Geol.* 97 (5), 1079–1100. doi:10.2113/gsecongeo.97.5.1079

Yang, K., and Scott, S. D. (2005). "Magmatic sources of volatiles and metals for volcanogenic massive sulfide deposits on modern and ancient seafloors: evidence from melt inclusions," in *Mineral deposit research: meeting the global challenge: proceedings of the eighth biennial SGA meeting beijing,*

China, 18–21 august 2005. Editors J. Mao and F. P. Bierlein (Berlin, Heidelberg: Springer Berlin Heidelberg), 715–718.

Yeats, C. J., Parr, J. M., Binns, R. A., Gemmell, J. B., and Scott, S. D. (2014). The SuSu knolls hydrothermal field, eastern Manus Basin, Papua New Guinea: an active submarine high-sulfidation copper-gold system. *Econ. Geol.* 109 (8), 2207–2226. doi:10.2113/econgeo.109.8.2207

Zellmer, K. E., and Taylor, B. (2001). A three-plate kinematic model for Lau Basin opening. *Geochem. Geophys. Geosyst.* 2 (5), GC000106. doi:10.1029/2000gc000106

Zwaan, F., and Schreurs, G. (2017). How oblique extension and structural inheritance influence rift segment interaction: insights from 4D analog models. *Interpretation.* 5 (1), SD119–SD138. doi:10.1190/int-2016-0063.1

Conflict of Interest: Nautilus Minerals provided in-kind donation of all geophysical data. JMP is employed fulltime by Nautilus Minerals Ltd. (now Deep sea Mining Finance); NJD conducted paid casual contract work for Nautilus Minerals Ltd. during his PhD.

The remaining authors declare that the research was conducted in the absence of any commercial or financial relationships that could be construed as a potential conflict of interest.